

The FAM83 family of proteins are anchors for Casein Kinase 1 isoforms through the *DUF1669* domain

Luke J Fulcher¹, Polyxeni Bozatzki¹, Theresa Tachie-Menson¹, Kevin Z L Wu¹, Timothy D Cummins¹, Joshua C Bufton³, Daniel M Pinkas³, Karen Dunbar¹, Sabin Shrestha¹, Nicola T Wood¹, Simone Weidlich¹, Thomas J Macartney¹, Joby Varghese¹, Robert Gourlay¹, David G Campbell¹, Kevin S Dingwell², James C Smith², Alex N Bullock³ and Gopal P Sapkota^{1*}

¹Medical Research Council Protein Phosphorylation and Ubiquitylation Unit, Dundee, Scotland, UK, ²The Francis Crick Institute, London, UK, ³Structural Genomics Consortium, University of Oxford, Oxford, UK.

*Address correspondence to g.sapkota@dundee.ac.uk

Abstract

The Casein Kinase 1 (CK1) family of Ser/Thr protein kinases are implicated in the regulation of many cellular processes, including cell cycle, circadian rhythm, Wnt and Sonic Hedgehog signalling. Regarded as constitutively active kinases, their regulation in cells is critically important but poorly understood. We report here that members of the FAM83 family of uncharacterized proteins are central regulators of CK1 isoforms in cells. The eight members of the FAM83 family (A-H) interact and co-localize with different CK1 α , α -like, δ and ϵ isoforms. We demonstrate that the interaction with CK1 isoforms is mediated through a number of residues within a conserved domain of unknown function, termed *DUF1669*, which characterises the FAM83 family. CK1-binding deficient mutants of FAM83 proteins interfere with the subcellular localization of CK1 isoforms as well as FAM83 proteins themselves and their cellular functions. We propose that *DUF1669* be renamed the *Polypeptide Anchor of CK1 (PACK1)* domain.

Introduction

The eight members of the FAM83 protein family are conserved in vertebrates but are poorly characterised. They share a conserved N-terminal *DUF1669* (domain of unknown function 1669) of ~300 amino acids and possess unique C-termini of variable lengths^{1,2}. The amino acid sequences of the FAM83 family members offer very few clues to their functions. The *DUF1669* domain contains a putative phospholipase D-like (PLD-like) catalytic motif, which is characterized by the presence of “HKD” residues in a “HxKxxxxD” sequence motif. Typically, two such motifs exist within each PLD protein and the two “HKD” motifs come together to form the catalytic core³. FAM83 proteins, on the other hand, have only one “HKD” motif, and the *H* residue within the motif is absent from all but FAM83D (also known as CHICA) (fig. S1). No PLD activity has yet been demonstrated for any FAM83 member⁴. Recent studies have implicated FAM83A and FAM83B in oncogenesis and resistance to tyrosine kinase inhibitors⁴⁻⁶. FAM83D has been reported to localise to the mitotic spindle and interact with the chromokinesin Kid, the microtubule binding protein HMMR and the light chain of the motor protein dynein (DYNLL1) to regulate mitosis^{7,8}. FAM83G (also known as PAWS1) interacts with SMAD1 and regulates transcription in BMP signalling and beyond². FAM83H has been reported to be mutated in Amelogenesis Imperfecta (AI) and mis-expressed in cancer⁹⁻¹¹. No functions have yet been reported for FAM83C, FAM83E or FAM83F. Despite the increasing evidence for diverse biological processes controlled by the FAM83 proteins, the precise molecular and biochemical roles of the FAM83 proteins, and in particular the *DUF1669* domain that characterises them, remain undefined.

To uncover potential roles of the FAM83 family and the *DUF1669* domain, we undertook a comprehensive proteomic approach. Many unique interactors of each of the FAM83 proteins were identified, perhaps reflecting their diverse sequence composition. However, Casein Kinase 1 (CK1) α , α -like, δ , and ϵ isoforms were identified as interactors of all of the FAM83 members, albeit with different affinities and specificities. These observations suggested that the *DUF1669* domain, which is conserved in all FAM83 members, might mediate the interaction with CK1 isoforms and that the FAM83 family of proteins are regulators of the CK1 isoforms in cells.

CK1 enzymes in vertebrates include the α , α -like, δ , ϵ , $\gamma 1$, $\gamma 2$, and $\gamma 3$ isoforms and all are Ser/Thr protein kinases. CK1 isoforms consist of a highly conserved N-terminal kinase domain with little homology elsewhere^{12, 13}. However, within the CK1 family, there is greater overall sequence homology between α/α -like isoforms, δ/ϵ isoforms, and $\gamma 1/\gamma 2/\gamma 3$ isoforms^{12, 13}. CK1 isoforms play fundamental roles in many aspects of cellular homeostasis, including cell cycle progression¹⁴, circadian rhythm¹⁵⁻¹⁷, survival^{18, 19}, DNA damage repair²⁰, membrane trafficking and integration of signalling processes¹²⁻¹⁴. Malfunction of CK1 isoforms have been linked to cancer¹³ and neurological pathologies²¹. Due to their spontaneous in vitro kinase activity against many substrates, CK1 isoforms are considered as constitutively active kinases in cells¹². Consistent with the large number of cellular processes influenced by CK1 isoforms, they have been reported to localise to many subcellular compartments, including the plasma membrane, cytoplasm, nucleus, actin cytoskeleton and mitotic spindle, and hundreds of putative substrates have been described^{12, 14, 22}. While the CK1 isoforms preferentially phosphorylate Ser/Thr residues within the consensus sequence pS/pT-X-X-S/T, in many cases CK1 isoforms phosphorylate residues without the need for the consensus motif, such as the phosphorylation of β -catenin on Ser⁴⁵¹². In some cases, acidic residues can substitute the need for the phospho-residues within the consensus motif¹². All of these studies indicate that the localisation, activity and substrate specificity of CK1 in cells are tightly regulated.

Interacting proteins that potentially regulate subcellular localisation, substrate accessibility, stability, and activity of CK1 isoforms remain elusive and poorly characterised. Thus far, two scaffold proteins, namely the centrosomal and Golgi N-kinase anchoring protein (CG-NAP; aka AKAP450) and the DEAD-box RNA helicase DDX3, have been implicated in the centrosomal localization of CK1 δ during cell cycle and Wnt-dependent phosphorylation of DVL by CK1 ϵ , respectively^{23, 24}. The potential existence of CK1 scaffolds in cells is supported by the A-kinase anchoring proteins (AKAPs), which are established scaffolds that regulate the activity and substrate specificity of Protein Kinase A (PKA; also known as cAMP-dependent kinase) by interacting with PKA and tethering it to distinct subcellular compartments²⁵.

Our data suggest that the *DUF1669* domain of the FAM83 family of proteins mediates the interaction with CK1 isoforms. FAM83 members localise to different subcellular

compartments and co-localize only with the CK1 isoforms that they interact with, and mutations within the *DUF1669* domain that abolish the interaction with CK1 interfere with the localisation of both the FAM83 members themselves and CK1 isoforms. We hypothesise that FAM83 members regulate the function of CK1 isoforms in cells through their association. We are investigating whether the interaction regulates CK1 activity, stability, substrate specificity and subcellular localisation.

Results

The FAM83 members interact with CK1 isoforms.

The FAM83 family of proteins comprise a conserved domain of unknown function, termed *DUF1669*, at their N-termini, while the rest of the protein varies in length and is not conserved between members (Fig. 1A; fig. S1). In order to investigate the roles of the FAM83 family of proteins, we generated human embryonic kidney HEK-293 cells stably integrated with a single copy of each FAM83 gene tagged at the N-terminus with green fluorescent protein (GFP) under a tetracycline (Tet)-inducible promoter. In these cells, doxycycline treatment induced the expression of the respective FAM83 protein in a time-dependent manner, with detectable amounts observed as early as 30 min after doxycycline treatment (Fig. 1B). Similarly, we generated U2OS osteosarcoma cells stably integrated with a single copy of each FAM83 gene tagged at the C-terminus with green fluorescent protein (GFP), except FAM83B, which did not express. All FAM83 proteins displayed robust expression following 24 h treatment with doxycycline (Fig. 1C). In both cases, cells stably integrated with GFP alone under the Tet-inducible promoter were used as controls.

We employed mass-spectrometry to identify interactors of all the FAM83 proteins from the Tet-inducible HEK-293 and U2OS cells described above (Fig. 1, B and C). Following 24 h induction with doxycycline, cell extracts expressing GFP control (HEK-293 & U2OS) and either N- (HEK-293) or C-terminal (U2OS) GFP-tagged FAM83 proteins were subjected to GFP-trap immunoprecipitation (IP) and the IPs were resolved by SDS-PAGE (fig. S2, A and B). The gel sections covering the entire lane for each sample were excised and digested with trypsin (fig. S2, A and B). The resulting peptides were identified using mass spectrometry. In addition to confirming the identity of the respective FAM83 proteins in each lane, consistent with previously reported

observations we identified SMAD isoforms in GFP-FAM83G IPs² and DYNLL1 and HMMR in GFP-FAM83D IPs^{7,8} (fig S2, A and B). Under these conditions, at least one or more of CK1 α , α -like, δ and ϵ isoforms were identified as interactors of every FAM83 family member, regardless of the positioning of the GFP-tag and cell lines employed (Fig. 2A). Analysis of the top 3 precursor ion intensities of the individual CK1 isoforms bound to each GFP-FAM83 protein from HEK293 extracts revealed that while all FAM83 members interact with CK1 α and α -like, only FAM83A, FAM83B, FAM83E and FAM83H interact with CK1 δ and CK1 ϵ (Fig. 2A). Similar patterns in spectral intensities were observed for CK1 α , CK1 δ and CK1 ϵ bound to FAM83-GFP proteins from U2OS cell extracts, while CK1 α -like was not detected in FAM83C, FAM83D and FAM83H IPs (Fig. 2A). Although we observed differences in spectral intensities for each isoform associated with different FAM83 members, it is difficult to interpret these differences as the relative amount of FAM83 protein in each lane is quite different as judged by the intensity of Coomassie stains (fig S2, A and B).

In order to verify the interactions between FAM83 members and CK1 isoforms, GFP-FAM83A-H or control GFP IPs from HEK-293 extracts were probed for co-precipitation of endogenous CK1 α , δ and ϵ isoforms. The relative amounts of FAM83 proteins in IPs varied in that the amounts of FAM83B and FAM83D, both in extracts and IPs, were lower when compared with other FAM83 members (Fig. 2B; fig. S3A). Under these conditions, in agreement with the proteomic data above, all GFP-FAM83 members, but not GFP control, appeared to interact with CK1 α (Fig. 2B). We observed that FAM83B, FAM83E, FAM83G and FAM83H appear to interact with CK1 α with slightly higher extents than FAM83A, FAM83C, FAM83D, and FAM83F (Fig. 2B). Endogenous CK1 δ and ϵ were mainly detected in FAM83B, FAM83E and FAM83H IPs, while CK1 ϵ was also observed in FAM83A IPs (Fig. 2B). In line with the proteomic data, endogenous SMAD1 co-precipitated with only FAM83G, while endogenous HMMR and DYNLL1 co-precipitated exclusively with FAM83D (Fig. 2B).

We next sought to verify endogenous interactions between some FAM83 members and CK1 α and ϵ . For this, in the absence of robust immunoprecipitating antibodies against FAM83 members, we exploited CRISPR/Cas9 genome editing technology to introduce GFP-tag knockins at the endogenous FAM83B (N-terminus) and FAM83G (C-terminus)

gene loci in HaCaT keratinocytes and U2OS cells respectively. The disappearance of the endogenous FAM83B and FAM83G signals at the predicted molecular weights upon GFP-tag knockins and their concomitant appearance at higher molecular weights equivalent to the added GFP, in combination with genomic DNA sequencing, confirmed the insertion of the GFP-tag at the appropriate loci (fig. S3B). Using these cells, we detected endogenous CK1 α in IPs of both ^{GFP/GFP}FAM83B and FAM83G^{GFP/GFP}, while CK1 ϵ was detected in ^{GFP/GFP}FAM83B IPs only (Fig. 2, C and D). Neither of the CK1 isoforms was detected in GFP IPs from wild type cells (Fig. 2, C and D). Furthermore, we detected endogenous FAM83G and FAM83H proteins in CK1 α IPs from U2OS cell extracts but not in pre-immune IgG control IPs (Fig. 2E). The CK1 branch of the human protein kinases also includes CK1 γ 1, γ 2, and γ 3 isoforms, tau-tubulin kinases (TTBK) 1 & 2 and vaccinia related kinases (VRK) 1-3²⁶. In cell extracts, under co-expression conditions in which FAM83G interacts with CK1 α , we were unable to detect interactions between FAM83G and either TTBK2 or CK1 γ (Supplementary Fig. 4A). This, together with the proteomic data, suggests that FAM83 members interact only with one or more of CK1 α , α -like, δ and ϵ isoforms but not with other members of the CK1 family.

The *DUF1669* domain of FAM83 members is sufficient in mediating the interaction with CK1 isoforms.

The conserved *DUF1669* domain unites the FAM83 family of proteins (Fig. 1A; fig S1). We postulated that the *DUF1669* domain might mediate the interaction with CK1 isoforms. To map the minimal domain within FAM83 proteins that mediates the interaction with CK1 isoforms, we co-expressed Myc-tagged FAM83G fragments with full-length HA-CK1 α in FAM83G^{-/-} U2OS cells²⁷ and performed co-IP experiments (Fig. 3A). HA-CK1 α IPs were able to co-precipitate only those FAM83G fragments that contained residues 165-307 within the *DUF1669* domain (Fig. 3A). We asked whether the interaction between the *DUF1669* domain and CK1 is direct by performing an in vitro binding assay between the recombinant 6xHis-FAM83A(124-304) fragment and the kinase domain of CK1 ϵ . We observed a robust interaction between the two, indicating a direct association (Fig. 3B). To probe the CK1 isoform-specific nature of interaction of FAM83 members, we switched the *DUF1669* domain of FAM83G, which interacts only with CK1 α , with that of FAM83H, which interacts with both CK1 α and CK1 ϵ and tested the interactions in extracts. Interestingly, the *DUF1669*_H-FAM83G chimera was able to

interact with both CK1 α and CK1 ϵ , much like FAM83H (fig. S5), suggesting that the *DUF1669*_H domain is sufficient to mediate selectivity for CK1 isoforms.

A CK1 docking motif, including an F-X-X-X-F amino acid sequence, was identified in NFAT1 and PER1/2 proteins, and mutation of either phenylalanine residue abolished CK1 interactions²⁸. Interestingly, one such F-X-X-X-F motif is conserved within the *DUF1669* domain of all FAM83 proteins, while FAM83H has four²⁹ (fig. S1). To ask whether mutations within this conserved motif are sufficient to disrupt the CK1 interaction, we tested the ability of wild-type FLAG-FAM83G or FAM83G^{F296A}, FAM83G^{F300A} and FAM83G^{F296A/F300A} mutants overexpressed in FAM83G^{-/-} U2OS cells to interact with HA-CK1 α (Fig. 3C). While wild-type FAM83G interacted robustly with CK1 α , FAM83G^{F296A} and FAM83G^{F296A/F300A} mutants did not (Fig. 3C). Rather surprisingly, FAM83G^{F300A} interacted with CK1 α as robustly as wild-type FAM83G (Fig. 3C), suggesting the mode of CK1-interaction with FAM83 proteins might be different from NFAT1 and PER1/2 proteins, in which mutation of either F residue abolished CK1 association²⁸. Consistent with this notion, subsequent mutational scanning of conserved residues within the 165-307 region of FAM83G uncovered another mutation, D262A, which also abolished the interaction with CK1 α ³⁰.

Armed with the knowledge that FAM83G^{D262A} and FAM83G^{F296A} mutants both abolish the interaction with CK1 α , we asked whether equivalent mutations on other FAM83 members also abolish their association with CK1 α and CK1 ϵ isoforms. Thus, we mutated the FAM83G D²⁶² and F²⁹⁶ equivalent residues to Ala (referred to as D/A and F/A respectively) in FAM83E (D²⁴³ & F²⁷⁷), FAM83F (D²⁵⁰ & F²⁸⁴) and FAM83H (D²³⁶ & F²⁷⁰). Then, we expressed either wild-type GFP-FAM83E-H or GFP-FAM83E-H^{D/A} and GFP-FAM83E-H^{F/A} mutants in U2OS cells and tested their ability to co-precipitate endogenous CK1 α or CK1 ϵ isoforms (Fig. 3D). In comparison to wild-type FAM83E-H, both the D/A and F/A mutations attenuated the interaction with CK1 α and CK1 ϵ isoforms (Fig. 3D). These observations suggest that the interaction between the *DUF1669* domain and CK1 isoforms may be mediated through a conserved structural motif surrounding the equivalent of residues D²⁶² and F²⁹⁶ in FAM83G. Consistent with previous observations (Fig. 2, B to D), while FAM83E and FAM83H bound both CK1 α and CK1 ϵ , FAM83F and FAM83G bound only CK1 α (Fig. 3D).

FAM83 proteins and CK1 α co-localize in cells.

Given the interaction between all of the FAM83 members and CK1 α in cell extracts, we sought to investigate whether they also interact with CK1 α in cells. We transfected mCherry-CK1 α into U2OS Flp-In T-Rex cells expressing N-terminal GFP-FAM83A-H under the control of the Tet-inducible promoter. Upon Tet-induction, we observed overlapping co-localization of every GFP-FAM83 member with mCherry-CK1 α (Fig. 4), with a distinct pattern of subcellular localization for each. Pan-cellular staining was observed for both GFP-FAM83A and GFP-FAM83B, along with additional perinuclear punctate structures (FAM83A) and membrane punctate structures (FAM83B) (Fig. 4). GFP-FAM83C displayed distinct fibrous patterns of fluorescence in the cytoplasm and in the vicinity of membrane ruffles, suggesting possible co-localization with cortical actin stress fibres (Fig. 4). GFP-FAM83D displayed cytoplasmic staining, with some punctate staining in the nucleus (Fig. 4). FAM83D has previously been reported to localize on the spindle apparatus during mitosis^{7,8}. Cytoplasmic as well as strong perinuclear staining was observed for GFP-FAM83E (Fig. 4). GFP-FAM83F displayed strong plasma membrane localization, while some staining was also observed in the cytoplasm and nucleus (Fig. 4). As reported previously², GFP-FAM83G localized mainly to the cytoplasm but some nuclear staining was also noted (Fig. 4). GFP-FAM83H displayed primarily cytoplasmic, and few nuclear, punctate fluorescence patterns (Fig. 4), like the patterns described previously for FLAG-FAM83H overexpressed in HCT116 cells¹⁰. GFP only control displayed predominantly nuclear staining, which did not overlap with mCherry-CK1 α , which displayed a pan-cellular staining (fig. S6). Furthermore, mCherry-CK1 α alone control displayed a pan cellular staining pattern (fig. S6). These observations describe the subcellular localization profiles for all FAM83 members and demonstrate that every member co-localizes with CK1 α .

In order to confirm whether endogenous CK1 α also displayed similar overlapping subcellular distribution with FAM83 members, we undertook further co-staining experiments with anti-CK1 α in U2OS cells stably expressing GFP control (nuclear), GFP-FAM83B & GFP-FAM83F (predominantly located on the plasma membrane) and GFP-FAM83H (cytoplasmic and nuclear speckles). No overlapping fluorescence was detected between endogenous CK1 α and GFP, which was employed as a negative

control (Fig. 5). Overlapping plasma membrane and perinuclear staining was observed for endogenous CK1 α and GFP-FAM83B (Fig. 5). Likewise, strong overlapping plasma membrane staining was observed for endogenous CK1 α and GFP-FAM83F (Fig. 5). GFP-FAM83H and endogenous CK1 α displayed overlapping staining in cytoplasmic and nuclear speckles (Fig. 5). Collectively these observations demonstrate that upon overexpression, each FAM83 protein is capable of relocating endogenous CK1 α to distinct subcellular compartments that they reside in.

Selectivity of association between FAM83 proteins and specific CK1 isoforms persists in cells.

Our data above show that all FAM83 members interact and co-localize with both overexpressed and endogenous CK1 α , but only FAM83A, FAM83B, FAM83E and FAM83H also interact with the CK1 δ and CK1 ϵ isoforms. To ask whether this CK1 isoform binding repertoire is maintained in cells, we compared the subcellular co-localizations of CK1 α and CK1 ϵ with FAM83F, a selective interactor of CK1 α , and FAM83H, an interactor of both CK1 α and CK1 ϵ . First, GFP-FAM83F or GFP-FAM83H was co-expressed in U2OS cells with either mCherry-tagged CK1 α or CK1 ϵ isoform. As observed earlier (Fig. 4 and 5), we found that both GFP-FAM83F and GFP-FAM83H displayed overlapping fluorescence with mCherry-CK1 α , at the plasma membrane and cytoplasmic speckles respectively (Fig. 6A). In contrast, GFP-FAM83H, but not GFP-FAM83F, also co-localized with mCherry-CK1 ϵ at these cellular sites (Fig. 6A). Next, we sought to verify whether the binding specificity of GFP-FAM83F and GFP-FAM83H extended to endogenous CK1 α and CK1 ϵ . In WT U2OS cells, endogenous CK1 α and CK1 ϵ both displayed pan-cellular distribution, with some speckle-like structures also visible (Fig. 6B). In U2OS cells expressing GFP-FAM83F, we observed overlapping plasma membrane co-localisation only with endogenous CK1 α but not with CK1 ϵ (Fig. 6B). In contrast, in U2OS cells expressing GFP-FAM83H, we observed overlapping cytoplasmic and nuclear speckle staining patterns with both endogenous CK1 α and CK1 ϵ (Fig. 6B). These data are consistent with our observations with over-expressed mCherry-CK1 α and mCherry-CK1 ϵ above (Fig. 6A). Collectively, these data recapitulate in cells the distinct sets of interactions that we observed between FAM83 members and CK1 isoforms from the proteomic data (Fig. 2A).

The subcellular localization of FAM83C is determined by its association with CK1.

We next asked whether the interaction between the various CK1 isoforms and FAM83 family members was important for their subcellular localizations. For this purpose, we chose GFP-FAM83C, because of its distinct cortical fibre-like subcellular localization pattern (Fig. 4). First, we confirmed in extracts that only wild-type GFP-FAM83C co-precipitated HA-tagged CK1 α while GFP-FAM83C^{D259A} and GFP-FAM83C^{F293A} mutants and control GFP did not (Fig. 7A). Next, we co-transfected U2OS cells with mCherry-CK1 α and either wild-type GFP-FAM83C or the CK1-interaction deficient GFP-FAM83C^{D259A} and GFP-FAM83C^{F293A} mutants and examined their subcellular localization by fluorescence microscopy. GFP-FAM83C and mCherry-CK1 α fluorescence co-localized along fibrous structures (Fig. 4 and 7B), while in contrast, GFP-FAM83C^{D259A} and GFP-FAM83C^{F293A} mutants displayed predominantly cytoplasmic, slightly distorted fibrous fluorescence patterns, which did not overlap with mCherry-CK1 α fluorescence (Fig. 7B). Interestingly, the fluorescence pattern for mCherry-CK1 α was distinctly different when it was co-expressed with WT-FAM83C compared to the CK1 α -interaction deficient mutants, suggesting that the interaction between FAM83C and CK1 α could determine the subcellular co-localization of both FAM83C and CK1 α . GFP-FAM83C alone expressed in U2OS cells displayed a fibrous staining, while mCherry-CK1 α alone displayed a pan-cellular staining (Fig. 7B).

FAM83H co-localizes with, and in part determines the subcellular localization of, endogenous CK1 α and CK1 ϵ isoforms.

We have shown that FAM83H displays distinct punctate fluorescence patterns when overexpressed in U2OS cells (Fig. 4 to 6). We generated FAM83H^{-/-} U2OS cells using CRISPR/Cas9 genome editing technology and asked whether endogenous CK1 α co-localizes with FAM83H that is restored in these cells. In FAM83H^{-/-} cells, CK1 α was primarily cytoplasmic with few perinuclear puncta. Upon restoration of GFP-FAM83H, pan-cellular punctate staining for both GFP-FAM83H and endogenous CK1 α was observed (Fig. 8A). While the majority of GFP-FAM83H puncta overlapped with endogenous CK1 α staining, suggesting robust co-localization, the non-overlapping GFP-FAM83H and CK1 α puncta suggest that both FAM83H and CK1 α exist in complexes with other CK1 isoforms (α -like, δ or ϵ) and FAM83 members respectively (Fig. 8A). In

contrast to GFP-FAM83H, the restoration of CK1-interaction deficient mutants, GFP-FAM83H^{D236A} and GFP-FAM83H^{F270A}, displayed cytoplasmic, non-punctate fluorescence that did not overlap with endogenous CK1 α staining (Fig. 8A). The intensity of CK1 α punctate staining in FAM83H^{-/-} cells and cells expressing CK1-binding mutants of FAM83H was lower compared to that seen in cells restored with wild-type GFP-FAM83H (Fig. 8A), suggesting that FAM83H expression potentially determines the CK1 α localization to the punctate structures. In order to quantify the co-localisation correlation between CK1 α and WT FAM83H, FAM83H^{D236A} or GFP-FAM83H^{F270A}, the fluorescence intensities were measured for the two channels by excluding the background noise and analysed using Pearson correlation coefficient as a measure of intensity correlation between the two channels. Consistent with co-localization data above, a positive correlation was observed for co-localisation of endogenous CK1 α and WT FAM83H (0.7523), whereas no significant co-localisation correlation was observed between CK1 α and the FAM83H^{D236A} (0.001504) or GFP-FAM83H^{F270A} (0.001504) mutants (Fig. 8B). Overlapping fluorescence observed with anti-CK1 α immunostaining and mCherry-CK1 α confirmed the selectivity and the applicability of the anti-CK1 α antibody for immunofluorescence (fig. S8A). Rescue with wild-type or mutant GFP-FAM83H constructs in FAM83H^{-/-} U2OS cells was confirmed by Western blotting and suggested that the FAM83H amounts in these cells were substantially higher than the endogenous FAM83H seen in wild type U2OS cells (Fig. 8C). In these cells, endogenous CK1 ϵ displayed similar immunostaining patterns to CK1 α and displayed significant co-localization correlation with WT FAM83H but not the FAM83H^{D236A} or GFP-FAM83H^{F270A} mutants (fig. S7).

The intrinsic catalytic activity of CK1 is not affected by FAM83 members and is not required for FAM83-CK1 association.

By associating with CK1 isoforms, it is possible that the FAM83 members could be substrates of CK1 isoforms or impact the intrinsic CK1 kinase activity. We set up an in vitro CK1 α kinase assay using recombinant FAM83A-H proteins expressed in *E. coli* as substrates. We observed that recombinant FAM83B, FAM83C and FAM83G were robustly phosphorylated by CK1 α , while other FAM83 members were phosphorylated poorly (Fig. 9A). The precise CK1 phosphorylation sites on most FAM83 proteins have not been mapped and whether these phosphorylation events occur in cells and their

potential functional consequences necessitate further investigation. Furthermore, the results should be considered carefully given the poor purity of some of the recombinant FAM83 proteins (Fig. 9A) and the absence in recombinant FAM83 proteins of any putative priming phosphorylation of an optimal (pS-x-x-S/T) CK1 phosphorylation motif¹². Separately, however, we have shown that in vitro, CK1 α phosphorylates FAM83G only on Ser⁶¹⁴ but this phosphorylation does not appear to alter the regulation of axis duplication in *Xenopus* embryos by FAM83G while its association with CK1 is essential³⁰.

In order to test whether the intrinsic catalytic activity of CK1 α was affected by FAM83 association, we performed an in vitro CK1 α kinase assay with increasing concentrations of an optimized CK1 peptide substrate (CK1tide), and evaluated whether addition of equimolar amounts of either WT or CK1-interaction-deficient mutant (F296A/F300A; FF/AA) of FAM83G altered the rate of CK1 α catalysis or its Michaelis constant (Km) against the CK1tide substrate. The intrinsic CK1 α catalytic activity against CK1tide was not significantly altered by the addition of either WT or the FF/AA mutant of FAM83G at all CK1tide concentrations tested, suggesting that the intrinsic CK1 α kinase kinetics are unaffected by FAM83G (Fig. 9B). We also assessed whether the kinase activity of CK1 α was required for its association with FAM83 members. For this, we transiently co-expressed GFP-FAM83E, F, G or H with either mCherry-tagged WT CK1 α or the catalytically inactive CK1 α ^{N141A} mutant³¹ and performed co-IP interaction assays. Equal amounts of both WT CK1 α and the CK1 α ^{N141A} mutant were detected in IPs of FAM83E-H (Fig. 9C), suggesting that CK1 kinase activity is dispensable for the FAM83:CK1 interaction.

Discussion

The CK1 isoforms are known to control a myriad of cellular processes, yet how they are regulated in cells remains poorly defined. In this report, we identify the poorly characterised FAM83 family of proteins as interactors of CK1 α , α -like, δ , and ϵ isoforms in mammalian cells. This interaction is mediated through the conserved *DUF1669* domain, with differences in affinity and isoform-selectivity also observed. Critically, we

show that FAM83 proteins display unique subcellular distribution, which overlaps with the specific CK1 isoforms that they associate with. Point mutations within the *DUF1669* domains of FAM83 proteins that abolish CK1 association disrupt not only the co-localization of FAM83 members with specific CK1 isoforms in cells, but also the subcellular localization of the respective FAM83 members themselves. Our findings imply that the *DUF1669* domain of FAM83 proteins serves as an anchor for CK1 α , α -like, δ and ϵ isoforms for their mobilization into specific cellular compartments and potentially their association with unique substrates, perhaps similar to the A-kinase anchoring proteins (AKAPs) that serve to localize protein kinase A to its substrates to streamline signal transduction²⁵. Unlike AKAPs, which bind the regulatory domain of PKA, the *DUF1669* domain of FAM83 proteins appears to associate directly with the kinase domain of CK1 isoforms independent of CK1 catalytic activity. There are many other examples of the crucial roles that scaffolding and anchoring proteins play in organizing and streamlining signal transduction in cells³²⁻³⁵. The scaffold protein TPX2, for example, serves to recruit Aurora Kinase A to the mitotic spindle, and activates the kinase allosterically³⁶. In our case, however, we show that FAM83G does not appear to influence the intrinsic catalytic activity of CK1 α . Because some FAM83 members appear to be substrates for CK1 isoforms, at least in vitro, future work will establish whether there are roles for some FAM83 proteins as substrates of CK1. The *DUF1669 domain* contains a pseudo-PLD-like catalytic motif, which has clearly evolved to become a binder for CK1. Hence, there could very well be features within the *DUF1669* domain of FAM83 proteins that still harbour certain pseudo-PLD roles, such as binding to specific phospho-lipids, which might regulate CK1 binding. Future work will unravel these fascinating possibilities that might explain the specificity and affinity with which FAM83 members bind different CK1 isoforms.

Precisely how FAM83 members impact the diverse functions of CK1 isoforms in cells is largely unclear, but we are beginning to uncover some of these roles. We have established that FAM83G is a critical mediator of Wnt signalling in human cells and *Xenopus* embryos³⁰. Crucially, we showed that unlike wild-type FAM83G, two mutants incapable of interacting with CK1 α are unable to activate Wnt signalling or induce axis duplication in *Xenopus* embryos³⁰. Similarly, a recent report suggested that FAM83H and SON recruit CK1 to nuclear speckles³⁷. From our proteomic data, it is evident that each FAM83 member interacts with unique proteins in addition to the CK1 isoforms.

Future investigations will establish whether FAM83 proteins individually recruit distinct sets of substrates to specific CK1 isoforms. Furthermore, by controlling the localization of CK1 isoforms, different FAM83 proteins might be primed to streamline diverse signal transduction processes downstream of CK1. Future efforts will aim to establish precisely which CK1 substrates are regulated by individual FAM83 members. Additionally, global phospho-proteomic approaches in cells devoid of individual FAM83 members generated by genome editing techniques will chart potential substrate maps for CK1 isoforms.

Given the involvement of CK1 isoforms in a wide-range of cellular processes, it is no surprise that their mis-regulation has been linked to cancers as well as neurological disorders^{14, 21}. The pleiotropic nature of CK1 function in regulating many cellular processes, combined with poor understanding of its regulation, has limited the exploration of CK1 for therapeutics. Nonetheless, several potent inhibitors of CK1 isoforms have been developed; including CKI-7, IC261, D4476, PF-670462 and PF-4800567, although they all suffer from selectivity issues, with off-target effects related to other CK1 isoforms and protein kinases³⁸⁻⁴². Our findings clearly place the FAM83 proteins at the helm of CK1 regulation in cells. Therefore, understanding the molecular bases for FAM83:CK1 association may provide us with unique opportunities to target and disrupt this association with small molecules, which could prove to be useful in targeting specific CK1 isoforms in desired cellular compartments.

In light of our data that clearly demonstrates that the *DUF1669* domain is responsible for facilitating the interaction between FAM83 members and CK1 isoforms, we propose that the *DUF1669* be renamed Polypeptide Anchor of CK1 (PACK1) domain. Co-crystallization of the PACK1 domain with CK1 isoforms will potentially reveal how CK1 interaction specificity and affinity is determined for each FAM83 member.

Materials and Methods

Plasmids

Recombinant DNA procedures were performed using standard protocols as described previously^{2, 43}. Human FAM83A-H genes or appropriate mutants were sub-cloned into pcDNA5-FRT/TO vectors with a Green Fluorescence Protein (GFP) tag at either N- or the C-terminus or mCherry tag at the N-terminus. All constructs are available to request

465 from the MRC-PPU reagents webpage (<http://mrccpureagents.dundee.ac.uk>) and the
 466 unique identifier (DU) numbers indicated above provide direct links to cloning strategy
 467 and sequence information. The following constructs were generated: pcDNA5-FRT/TO
 468 GFP-FAM83A (DU44235), pcDNA5-FRT/TO GFP-FAM83B (DU44236), pcDNA5-
 469 FRT/TO GFP-FAM83C (DU42473), pcDNA5-FRT/TO GFP-FAM83D (DU42446),
 470 pcDNA5-FRT/TO GFP-FAM83E (DU44237), pcDNA5-FRT/TO GFP-FAM83F
 471 (DU44238), pcDNA5-FRT/TO GFP-FAM83G (DU33272), pcDNA5-FRT/TO GFP-
 472 FAM83H (DU44239), pcDNA5-FRT/TO GFP-FAM83C (D259A) (DU28479), pcDNA5-
 473 FRT/TO GFP-FAM83C (F293A) (DU28480), pcDNA5-FRT/TO GFP-FAM83E (D243A)
 474 (DU28481), pcDNA5-FRT/TO GFP-FAM83E (F277A) (DU28482), pcDNA5-FRT/TO
 475 GFP-FAM83F (D250A) (DU28268), pcDNA5-FRT/TO GFP-FAM83F (F284A)
 476 (DU28488), pcDNA5-FRT/TO GFP-FAM83G (D262A) (DU28476), pcDNA5-FRT/TO
 477 GFP-FAM83G (F296A) (DU28477), pcDNA5-FRT/TO GFP-FAM83H (D236A)
 478 (DU28428), pcDNA5-FRT/TO GFP-FAM83H (F270A) (DU28487), pcDNA5-FRT/TO
 479 mCherry-CK1 α (DU28407), pcDNA5-FRT/TO mCherry-CK1 α (N141A) (DU28839),
 480 pcDNA5-FRT/TO GFP-FAM83H(M1-L284)-FAM83G(S311-P823) (DU28683), pcDNA5-
 481 FRT/TO GFP-FAM83G(M1-V310)-FAM83H(V285-K1179) (DU28688), pcDNA5-FRT/TO
 482 FAM83A-GFP (DU42864), pcDNA5-FRT/TO FAM83B-GFP (DU42833), pcDNA5-
 483 FRT/TO FAM83C-GFP (DU42825), pcDNA5-FRT/TO FAM83D-GFP (DU42835),
 484 pcDNA5-FRT/TO FAM83E-GFP (DU42826), pcDNA5-FRT/TO FAM83F-GFP
 485 (DU42832), pcDNA5-FRT/TO FAM83G-GFP (DU42816), pcDNA5-FRT/TO FAM83H-
 486 GFP (DU42865), pcDNA5-FRT/TO GFP only (DU41455), pcDNA5-FRT/TO GFP-
 487 FAM83H (F274A) (DU28658), pcDNA5-FRT/TO GFP-FAM83H (F270/274A) (DU28182),
 488 pcDNA5-FRT/TO FLAG-FAM83G (DU), pcDNA5-FRT/TO FLAG-FAM83G (F296A)
 489 (DU28024), pcDNA5-FRT/TO FLAG-FAM83G (F296A/F300A) (DU28026), pcDNA5-
 490 FRT/TO FLAG-FAM83G (F300A) (DU28025), pCS2+ HA-CK1 α (DU28216), pCMV5-
 491 FLAG TTBK2 (DU19028), pCMV-FLAG-CK1 γ (DU5580), pCS2+ HA CK1 δ (DU28189),
 492 pcDNA5-FRT/TO mcherry-CK1 ϵ (DU28406). Myc-xFAM83G constructs have been
 493 described previously ²⁷. For CRISPR/Cas9 gene editing, pBABED P U6 FAM83H KO
 494 sense gRNA (DU52010), pX335-CAS9-D10A FAM83H KO antisense gRNA (DU52026),
 495 pBABED P U6 FAM83G KI sense gRNA (DU48793), pX335-CAS9-D10A FAM83G KI
 496 antisense gRNA (DU48826), pEX-K4 FAM83G Cter GFP donor (DU48585), pBABED P
 497 U6 FAM83B KI sense gRNA (DU54494), pX335-CAS9-D10A FAM83B KI antisense
 498 gRNA (DU54054), and pEX-K4 FAM83B Nter GFP donor (DU54547) were generated

and used. Constructs were sequence-verified by DNA Sequencing Service, University of Dundee (<http://www.dnaseq.co.uk>). For plasmid amplification, 1 µl of the plasmid was transformed into 10 µl of *E. coli* DH5α competent bacteria (Invitrogen) on ice, incubated at 42°C for 45 s, then on ice for 2 min, before plating on LB-agar medium plate containing 100 µg/ml ampicillin. Plates were inverted and incubated for 16 h at 37°C. A single colony was picked and used to inoculate 250 ml of LB medium containing 100 µg/ml ampicillin and cultures were grown for 18 h at 37°C in a shaker (Infors HT). Plasmid DNA was purified using a Qiagen midi-prep kit as per the manufacturer's instructions. The isolated DNA yield was subsequently analysed using a Nanodrop 1000 spectrophotometer (Thermo Scientific).

Antibodies

Rabbit anti-GAPDH (cat.: 14C10), anti-CK1δ (cat.: 12417S), and anti-CK1ε (cat.: 12448) were from Cell Signalling Technology (CST). Rat anti-GFP for detection of endogenous GFP tags was from Chromotek (cat.: 3H9). Anti-CK1α (cat.: A301-991A) and anti-FAM83H (cat.: A304-327A) were from Bethyl. Anti-DYNLL1 (EP1660Y) and anti-FAM83B (cat.: 153829) were from Abcam. Anti-HMMR (cat.: ABC323) was from Millipore. Sheep anti-PAWS1/FAM83G (S876C, 3rd bleed), anti-FAM83H (SA273, 4th bleed), anti-GFP (S268B, 2nd bleed) and anti-SMAD1 (S618C, 3rd bleed) were generated by the Division of Signal Transduction Therapy (DSTT), University of Dundee^{2, 44}. anti-FLAG M2-Peroxidase (HRP) (cat.: A8592) and anti-c-myc-HRP (cat.: A5598) were from Sigma and Anti-HA-HRP (cat.: 11667475001) was from Roche. For Immunofluorescence, anti-CK1-alpha (C-19 Santa Cruz Biotechnology) and anti-CK1-epsilon (HPA026288 Sigma) were used. For signal amplification, AlexaFluor-594 donkey anti-goat IgG (H+L) (A11058 Life Technologies), AlexaFluor-594 goat anti-rabbit IgG (H+L) (A11012 Invitrogen™ Molecular Probes™) and AlexaFluor-488 donkey anti-rabbit IgG (H+L) (A21206, Life Technologies) were employed.

Cell Culture

Human osteosarcoma U2OS, Human keratinocyte HaCaT, Flp-In T-Rex U2OS and human embryonic kidney HEK293, and retroviral production HEK293(FT) cell lines were grown in Dulbecco's Modified Eagles Medium (DMEM; Gibco) containing 10% (v/v) Foetal Bovine Serum (FBS; Hyclone), penicillin (100 U/ml; Lonza), streptomycin (0.1

mg/ml; Lonza) and L-glutamine (2 mM; Lonza), and cultured at 37°C, 5% CO₂ in a humidified incubator. Cells were exposed to different stimuli and compounds as described in the appropriate figure legends prior to lysis. For transient transfections, cells were transfected for 24 h with 2 µg (per 10 cm-dish), or 500 ng (per 6-well dish with coverslips) cDNA, in serum free OptiMem (Gibco) with the transfection reagent polyethylenimine (PEI) as described previously⁴³.

Generation of Stable Flp-In T-Rex Cell Lines

The Flp-In T-Rex U2OS or HEK293 cells were transfected with the N- or C-terminal GFP-tagged FAM83A-H or GFP alone packaged onto pcDNA5-FRT/TO vector together with the Flp recombinase pOG44 (Invitrogen) in a ratio of 1 µg : 9 µg as described previously^{2, 45}. Briefly, plasmids were diluted in 1 ml OptiMem (Gibco), 20 µl of 1 mg/ml polyethylenimine (PEI) was added, the mix vortexed and left at room temperature for 15 min and added dropwise to 10 cm dish of target cells in 10 ml complete medium. 24 h post-transfection, cells were selected in media containing hygromycin (50 µg/ml) and blasticidin (15 µg/ml). Resistant cells were grown up to confluency, tested for doxycycline-induced expression of GFP-tagged proteins and used in subsequent experiments.

Generation of FAM83G^{GFP/GFP} and GFP/GFP^{FAM83B} knock-in cells using CRISPR/CAS9

U2OS and HaCaT cells were transfected with vectors encoding a pair of guide RNAs (pBABED-Puro-sgRNA1 and pX335-CAS9-D10A-sgRNA2) targeting around the stop codon of FAM83G and the start codon of FAM83B (1 µg each), along with the respective donor plasmids carrying the GFP knockin insert and flanking homology arms (~500 bases) (3 µg each). 16 h post-transfection, cells were selected in puromycin (2 µg/ml) for 2 days. The transfection process was repeated one more time. GFP-positive cells were isolated by fluorescence-activated cell sorting (FACS) and single GFP-positive cell clones were plated on individual wells of two 96-well plates, pre-coated with 1% (w/v) gelatin as described previously⁴⁴. Viable clones were expanded, and the integration of GFP at the target locus was confirmed by Western blotting and genomic sequencing of the targeted locus. The DU identifier numbers for the plasmids listed above link the sequences for gRNA and donors with homology arms for each target.

Generation of FAM83G^{-/-} and FAM83H^{-/-} cells using CRISPR/CAS9

CRISPR/Cas9 mediated deletion of FAM83G/PAWS1 in U2OS cells was performed using Cas9 and a single gRNA targeting approach to delete exon 2 of the RefSeq gene for FAM83G (NM_001039999.2). Vectors containing the Cas9 and FAM83G targeting gRNA (ggaccgctccatcccgagctgg) were transfected into 1x10⁶ U2OS cells followed by selection with 2 ug/ml puromycin. Single cell sorting was used to isolate clone candidates, which were screened with Western blotting and confirmed by genomic sequencing. For FAM83H, U2OS cells were transfected with vectors encoding a pair of guide RNAs (pBABED-Puro-sgRNA1 and pX335-CAS9-D10A-sgRNA2) targeting the second exon of FAM83H (1 µg each). 16 h post-transfection, cells were selected in puromycin (2 µg/ml) for 2 days. The transfection process was repeated one more time. Cells were isolated by single-cell sorting and isolated clones were plated on individual wells of two 96-well plates, pre-coated with 1% (w/v) gelatin as described previously⁴⁴. Viable clones were expanded and successful knockout of FAM83H was confirmed by Western blotting and genomic sequencing of the targeted locus. The DU identifier numbers for the plasmids listed above link the sequences for gRNA for each target.

Cell Lysis and Immunoprecipitation

Cells were washed twice in ice-cold phosphate-buffered saline (PBS), before scraping on ice in lysis buffer (50mM Tris-HCl pH 7.5, 0.27 M sucrose, 150 mM NaCl, 1 mM EGTA, 1 mM EDTA, 1 mM sodium orthovanadate, 10 mM sodium β-glycerophosphate, 50 mM sodium fluoride, 5 mM sodium pyrophosphate, and 1% Nonidet P40 substitute), supplemented with 1X protease inhibitor cocktail (Roche). Cell extracts were either cleared and processed immediately, or snap frozen in liquid nitrogen, before storing at -80°C. Protein concentrations were determined in a 96-well format using Bradford protein assay reagent (Pierce).

For Immunoprecipitation (IP), clarified extracts were diluted in lysis buffer to typically 1-5 mg/ml. Input aliquots were taken, and lysates were incubated overnight at 4°C with protein G-sepharose beads coupled to the antibody of interest, on a rotating wheel. For anti-GFP IPs, GFP-trap beads (Chromotek) were used; for anti-FLAG IPs, FLAG-agarose beads (Sigma) were used. Following the incubation period, beads were pelleted and flow-through extracts collected. Beads were washed once in lysis buffer

supplemented with 250 mM NaCl and 2-3 times in lysis buffer. Beads were eluted in 1X SDS sample buffer, at 95°C for 5 min.

For mass-spectrometry IPs, cells were lysed in DSP crosslinking lysis buffer (40 mM HEPES pH 7.4, 120 mM NaCl, 1 mM EDTA, 10 mM sodium pyrophosphate, 50 mM sodium fluoride, 1.5 mM sodium orthovanadate, 1% (v/v) triton, 1X protease inhibitor cocktail (Roche), and 2.5 mg/ml DSP as described previously². Following lysis, lysates were incubated for 30 mins at 4°C, before quenching the crosslinking reaction by adding 1 M Tris-HCl pH 7.4 in a ratio of 1:4, and incubating at 4°C for a further 30 min. Lysates were clarified by centrifugation at 15000 rpm for 20 min and filtered through 0.45 µm filters (BioRad). Extracts were pre-cleared by incubating with Protein-G sepharose beads for 1 h at 4°C on a rotating wheel. Pre-cleared lysates were quantified using the Bradford method, and extracts incubated with GFP-trap beads (Chromotek) for 4 h at 4°C on a rotating wheel. Input and post-IP extract aliquots were taken for control blots. Beads were washed twice in lysis buffer supplemented with 250 mM NaCl, and three times in lysis buffer. 1X SDS sample buffer containing 0.1 M DTT was added to the beads (~50% slurry), and samples incubated at 37°C for 1 h. Samples were then boiled at 95°C for 5 min and eluted through SpinX columns (Corning).

Mass Spectrometry

The expression of GFP-tagged FAM83 proteins in stable Flp-In T-Rex HEK293 and U2OS cells was induced with 20 ng/ml doxycycline for 24 h prior to lysis. Proteins were affinity purified from clarified extracts by GFP-trap beads (ChromoTek) as described above. Purified proteins were resolved by 4-12% gradient SDS-PAGE, the gels were Coomassie stained and gel slices covering each lane were excised and trypsin digested. The peptides were subjected to mass spectrometric analysis performed by LC-MS-MS on a Linear ion trap-orbitrap hybrid mass spectrometer (Orbitrap-VelosPro, Thermo) coupled to a U3000 RSLC Hplc (Thermo). Peptides were trapped on a nanoViper Trap column, 2 cm x 100 µm C18 5 µm 100 Å (Thermo, 164564) then separated on a 15 cm Thermo EasySpray column (ES800) equilibrated with a flow of 300 nl/min of 3% Solvent B. [Solvent A: 2% Acetonitrile, 0.1% formic acid, 3% DMSO in H₂O; Solvent B: 80% acetonitrile, 0.08% formic acid, 3% DMSO in H₂O]. The elution gradient was as follows; Time(min):Solvent B(%); 0:3, 5:3, 45:35, 47:99, 52:99, 55:3, 60:3. Data were acquired in the data-dependent mode, automatically switching between MS and MS-MS acquisition.

Full scan spectra (m/z 400-1600) were acquired in the orbitrap with resolution R = 60,000 at m/z 400 (after accumulation to an FTMS Full AGC Target; 1,000,000; FTMS MSn AGC Target; 50,000). The 20 most intense ions, above a specified minimum signal threshold (2,000), based upon a low resolution (R=15,000) preview of the survey scan, were fragmented by collision induced dissociation and recorded in the linear ion trap (Full AGC Target; 30,000. MSn AGC Target; 5,000). Data files were analysed by Proteome Discoverer 2.0 (www.ThermoScientific.com), using Mascot 2.4.1 (www.matrixscience.com), and searching the SwissProt Human database. Scaffold Q/Q+S V4.4.7 (www.ProteomeSoftware.com) was also used to examine the Mascot result files. Allowance was made for the following fixed, Carbamidomethyl (C), and variable modifications, Oxidation (M), Dioxidation (M). Error tolerances were 10ppm for MS1 and 0.6 Da for MS2. Scaffold Q/Q+S V4.3 (U2OS) or V4.4.6 (HEK293) (www.ProteomeSoftware.com) was used to further analyse the data and obtain values for the Top 3 precursor ion intensities of each protein.

SDS-PAGE and Western Blotting

Reduced protein extracts (typically 10–20 µg protein) or IPs were resolved on either 8% (v/v) SDS-PAGE gels, or 4-12% NuPAGE bis-tris precast gradient gels (Invitrogen) by electrophoresis. Separated proteins were subsequently transferred onto polyvinylidene fluoride (PVDF) membranes (Millipore), before membranes were blocked in 5% (w/v) non-fat milk powder (Marvel) in TBS-T (50 mM Tris-HCl pH 7.5, 150 mM NaCl, 0.2% (v/v) Tween-20) and incubated overnight at 4°C in 5% milk TBS-T or 5% bovine serum albumin (BSA) TBS-T with the appropriate primary antibody. Membranes were then washed 3 X 10 min with TBS-T before incubating with HRP-conjugated secondary antibodies in 5% milk TBS-T for 1 h at room temperature. Membranes were then washed 3 X 10 min with TBS-T before detection with enhanced chemiluminescence reagent (Millipore) and exposure to medical-grade X-ray films (Konica Minolta), as described previously^{2, 46, 47}.

Fluorescence microscopy

Cells were plated on glass coverslips and treated/transfected as described above or in figure legends. Cells were washed twice in PBS, before being fixed either with methanol at -20°C for 2 min or 4% (w/v) paraformaldehyde (PFA) in 200 mM HEPES pH 7.4 for 20 min at RT. Cells fixed in methanol were washed three times in ice cold PBS after fixation

then blocked in 3% BSA/PBS + 0.01% Tween 20 on ice for 30 min. Cells fixed in PFA were washed twice with DMEM/10 mM HEPES followed by incubation in DMEM/10 mM HEPES for 10 min. Cells fixed in PFA were washed once in PBS and permeabilised for 3 min in 1.5 ml 0.2% NP40. Cells were then washed twice in PBS containing 1-3% (w/v) BSA, followed by incubation in PBS/BSA for 15 min. Where appropriate, coverslips were then incubated with primary antibody in PBS/BSA (typically at 1:50-1:500 dilution as stated) at 30-37°C for 1-1.5 h. Cells were washed for a minimum of 3 X 10 min in PBS/BSA or 3 X 5 min in PBS only on shaker. Coverslips incubated with secondary Alexa-Fluor conjugated antibody in PBS/BSA (1:300-500 dilution) and DAPI (1:500) (for methanol-fixed cells) for 30 to 60 min at RT in the dark. Coverslips were then washed for 3 X 10 min in PBS/BSA or 3 X 5 min in PBS, and mounted on glass microscopy slides using ProLong® Gold anti-fade reagent with DAPI (Life Technologies) or mounted using VECTASHIELD mounting solution (Vector Labs). Coverslips were sealed with clear nail varnish and left to dry overnight before analysis on a Nikon TiS inverted microscope, or a DeltaVision Imaging Systems (GE Healthcare). Images were processed using either NIS Elements (Nikon) and Adobe Photoshop, or softWoRx (GE Healthcare) and Omero⁴⁸.

Colocalization was assessed using the Pearson's correlation coefficient (PCC) as a measure of intensity correlation between the two channels. As explained by Adler and Parmryd⁴⁹, PCC is sensitive to the inclusion of background pixels. We therefore excluded background pixels by auto-thresholding each channel in the cytoplasmic region of interest using Otsu's method⁵⁰. Thresholding and PCC calculation were implemented in an ImageJ macro developed by G. Ball (Dundee) and is included as Supplementary method.

In vitro kinase assays:

25 µl reactions were set up using 200 ng of kinase (GST-CK1α), 2 µg of substrate (GST-FAM83A, C, D, E, F, or H, MBP-tagged FAM83B, or GST-FAM83G-6XHis in a buffer containing 50 mM Tris pH 7.5, 0.1 mM EGTA, 10 mM Magnesium acetate, 2 mM DTT and 0.1 mM [³²P]-ATP (~500 cpm/pmol). Assays were performed at 30°C for 30 min and stopped by addition of 9 µl of 4xSDS sample buffer with 5% β-mercaptoethanol and heating at 95°C for 5 min. The samples were resolved by SDS-PAGE and the gels were stained with Instant blue (Expedeon) and dried. Radioactivity was analysed by autoradiography. For peptide-based kinase assays, reactions were set up and

performed as described by Hastie *et al*⁵¹, using an optimised CK1 peptide substrate (CK1tide (KRRRALS*VASLPGL), where S* indicates phospho-Ser). Assays were performed in triplicates.

Protein expression, purification and in vitro binding:

The *DUF1669* domain of FAM83A (a.a. 122-304) and the kinase domain of human CK1 ϵ (a.a. 1-294) were expressed separately in *E. coli* strain BL21(DE3) R3-pRARE2 using the pNIC28-Bsa4 vector, which encodes for a N-terminal hexahistidine (6XHis) tag and TEV cleavage site. Cultures were grown at 37°C in LB medium supplemented with 50 µg/mL kanamycin and 34 µg/mL chloramphenicol to an OD of 0.6, before expression at 18°C overnight by induction with 0.4 mM isopropyl 1-thio- β -D-galactopyranoside. Cells were harvested by centrifugation at 5000 g and pellets resuspended in binding buffer (50 mM HEPES pH 7.5, 500 mM NaCl, 5% glycerol, 5 mM imidazole) supplemented with Calbiochem protease inhibitor set III. Cells were lysed by sonication before clarification of the lysate by centrifugation in a JA 25.50 rotor at 36,000 g. His-tagged proteins were immobilized on Ni-sepharose and bound proteins were eluted using step gradients of imidazole (50-250 mM). CK1 ϵ protein was cleaved with TEV protease overnight at 4°C and both 6xHis-FAM83A and CK1 ϵ were purified further by size exclusion chromatography using an S75 HiLoad 16/60 Superdex column equilibrated in buffer containing 50 mM HEPES pH 7.5, 300 mM NaCl, and 0.5 mM TCEP. Proteins were concentrated by centrifugal ultrafiltration using a 3 kDa molecular weight cut-off concentrator. Protein concentrations were determined by measuring absorbance at 280 nm. Protein purity of >95% was confirmed by SDS-PAGE and construct identities and tag cleavage were verified by mass spectrometry.

For in vitro binding assay, all proteins and Ni-sepharose were equilibrated in binding buffer (50 mM HEPES pH 7.5, 500 mM NaCl, 5% glycerol, 5 mM imidazole) prior to use. 300 µg 6xHis-FAM83A (aa122-304) was immobilised onto 200 µl Ni-sepharose and washed before addition of 100 µg CK1 ϵ . The Ni-sepharose was then washed with binding buffer and the flow through collected. Two 1 ml wash steps were performed using binding buffer before bound proteins were eluted with 1 ml binding buffer supplemented with 250 mM Imidazole. Fractions were run on a SDS-PAGE gel alongside the original protein solutions for molecular weight reference.

The recombinant proteins used in the in vitro kinase assays were purified by the Division of Signal Transduction Therapy (DSTT; University of Dundee) and the identities of the expressed proteins verified by mass spectrometry. Each protein has a unique identification number to request from the MRC-PPU Reagents website (<http://mrcpppureagents.dundee.ac.uk>) as follows: GST-FAM83A (DU24611), GST-FAM83C (DU28269), GST-FAM83D (DU28270), GST-FAM83E (DU28271), GST-FAM83F (DU28272), GST-FAM83H (DU28403) and GST-FAM83G (F296A/F300A) (DU28049). Briefly, the proteins were expressed in BL21(DE3) *E. coli* as described above and affinity purified using GSH-sepharose, Amylose-sepharose or Nickel-agarose columns as appropriate.

Statistical Analysis:

For kinase assays, GraphPad (Prism) was used to generate plots and analyse data by two-way ANOVA, from at least 3 biological replicates. A p-value of <0.05 was deemed significant.

For co-localisation studies, GraphPad (Prism) was used to generate boxplots and analyse data by one-way ANOVA and Dunnett's multiple comparison test to determine statistical significance. A p-value of <0.05 was deemed significant.

Acknowledgements:

We thank G. Ball (Dundee) for analysing fluorescence images and developing an Image J Macro for Pearson correlation coefficient experiments. We thank L. Fin, J. Stark and A. Muir for help with tissue culture, the staff at the Sequencing Service (School of Life Sciences, University of Dundee, UK) for DNA sequencing, and the protein & antibody production and cloning teams at the Division of Signal Transduction Therapy (DSTT; University of Dundee) coordinated by H. McLauchlan and J. Hastie. LJF, PB, TT-M are supported by the U.K. MRC PhD studentships. We would like to acknowledge the Dundee Imaging Facility, Dundee, for image analysis support, which is funded by the 'MRC Next Generation Optical Microscopy' award [MR/K015869/1]. LJF also receives funding from the Queens College Scholarship, University of Dundee. KW and KD are supported by MRC Career Development Fellowships. GPS is supported by the U.K. Medical Research Council (grant number MC_UU_12016/3) and the pharmaceutical

companies supporting the DSTT (Boehringer-Ingelheim, GlaxoSmithKline, Merck-Serono). JCS and KSD are supported by the Francis Crick Institute, which receives its core funding from Cancer Research UK (FC001157), the UK Medical Research Council (FC001157), and the Wellcome Trust (FC001157). ANB, JCB and DMP are supported by the SGC, which is a registered charity (number 1097737) that receives funds from AbbVie, Bayer Pharma AG, Boehringer Ingelheim, Canada Foundation for Innovation, Eshelman Institute for Innovation, Genome Canada, Innovative Medicines Initiative (EU/EFPIA) [ULTRA-DD grant no. 115766], Janssen, MSD, Merck KGaA, Novartis Pharma AG, Ontario Ministry of Economic Development and Innovation, Pfizer, São Paulo Research Foundation-FAPESP, Takeda and Wellcome [106169/ZZ14/Z].

Author contributions: LJF, PB, TTM, KW, KD, TDC and SS performed experiments, collected and analysed data and contributed to the manuscript. TJM designed strategies and developed methodologies for, and generated, all CRISPR/Cas9 knockin constructs. TJM, NTW and SW cloned genes and performed mutagenesis experiments. JV, RG and DGC performed mass-spectrometry experiments, collected and analysed data. JCB & DMP performed in vitro interaction between FAM83A-DUF1669 and CK1 ϵ and contributed to the composition of the manuscript. KSD, JCS & ANB contributed with data analysis and the composition of the manuscript. GPS conceived the project, analysed the data and wrote the manuscript.

References

1. Bartel, C.A., Parameswaran, N., Cipriano, R. & Jackson, M.W. FAM83 proteins: Fostering new interactions to drive oncogenic signaling and therapeutic resistance. *Oncotarget* (2016).
2. Herhaus, L. *et al.* USP15 targets ALK3/BMPRI1A for deubiquitylation to enhance bone morphogenetic protein signalling. *Open Biol* **4**, 140065 (2014).
3. Selvy, P.E., Lavieri, R.R., Lindsley, C.W. & Brown, H.A. Phospholipase D: enzymology, functionality, and chemical modulation. *Chem Rev* **111**, 6064-6119 (2011).
4. Lee, S.Y. *et al.* FAM83A confers EGFR-TKI resistance in breast cancer cells and in mice. *J Clin Invest* **122**, 3211-3220 (2012).
5. Cipriano, R. *et al.* FAM83B mediates EGFR- and RAS-driven oncogenic transformation. *J Clin Invest* **122**, 3197-3210 (2012).
6. Cipriano, R. *et al.* FAM83B-mediated activation of PI3K/AKT and MAPK signaling cooperates to promote epithelial cell transformation and resistance to targeted therapies. *Oncotarget* **4**, 729-738 (2013).

- 808 7. Dunsch, A.K. *et al.* Dynein light chain 1 and a spindle-associated adaptor
809 promote dynein asymmetry and spindle orientation. *J Cell Biol* **198**, 1039-
810 1054 (2012).
- 811 8. Santamaria, A., Nagel, S., Sillje, H.H. & Nigg, E.A. The spindle protein CHICA
812 mediates localization of the chromokinesin Kid to the mitotic spindle. *Curr*
813 *Biol* **18**, 723-729 (2008).
- 814 9. Kim, J.W. *et al.* FAM83H mutations in families with autosomal-dominant
815 hypocalcified amelogenesis imperfecta. *Am J Hum Genet* **82**, 489-494 (2008).
- 816 10. Kuga, T. *et al.* A novel mechanism of keratin cytoskeleton organization
817 through casein kinase Ialpha and FAM83H in colorectal cancer. *J Cell Sci* **126**,
818 4721-4731 (2013).
- 819 11. Lee, S.K. *et al.* FAM83H mutations cause ADHCAI and alter intracellular
820 protein localization. *J Dent Res* **90**, 377-381 (2011).
- 821 12. Venerando, A., Ruzzene, M. & Pinna, L.A. Casein kinase: the triple meaning of
822 a misnomer. *Biochem J* **460**, 141-156 (2014).
- 823 13. Schittek, B. & Sinnberg, T. Biological functions of casein kinase 1 isoforms
824 and putative roles in tumorigenesis. *Mol Cancer* **13**, 231 (2014).
- 825 14. Knippschild, U. *et al.* The casein kinase 1 family: participation in multiple
826 cellular processes in eukaryotes. *Cell Signal* **17**, 675-689 (2005).
- 827 15. Camacho, F. *et al.* Human casein kinase I delta phosphorylation of human
828 circadian clock proteins period 1 and 2. *FEBS Lett* **489**, 159-165 (2001).
- 829 16. Keesler, G.A. *et al.* Phosphorylation and destabilization of human period I
830 clock protein by human casein kinase I epsilon. *Neuroreport* **11**, 951-955
831 (2000).
- 832 17. Kloss, B. *et al.* The Drosophila clock gene double-time encodes a protein
833 closely related to human casein kinase I epsilon. *Cell* **94**, 97-107 (1998).
- 834 18. Stoter, M. *et al.* Inhibition of casein kinase I delta alters mitotic spindle
835 formation and induces apoptosis in trophoblast cells. *Oncogene* **24**, 7964-
836 7975 (2005).
- 837 19. Zilian, O. *et al.* double-time is identical to discs overgrown, which is required
838 for cell survival, proliferation and growth arrest in Drosophila imaginal discs.
839 *Development* **126**, 5409-5420 (1999).
- 840 20. Bischof, J. *et al.* CK1delta kinase activity is modulated by Chk1-mediated
841 phosphorylation. *PLoS One* **8**, e68803 (2013).
- 842 21. Perez, D.I., Gil, C. & Martinez, A. Protein kinases CK1 and CK2 as new targets
843 for neurodegenerative diseases. *Med Res Rev* **31**, 924-954 (2011).
- 844 22. Cheong, J.K. & Virshup, D.M. Casein kinase 1: Complexity in the family. *Int J*
845 *Biochem Cell Biol* **43**, 465-469 (2011).
- 846 23. Cruciat, C.M. *et al.* RNA helicase DDX3 is a regulatory subunit of casein kinase
847 1 in Wnt-beta-catenin signaling. *Science* **339**, 1436-1441 (2013).
- 848 24. Sillibourne, J.E., Milne, D.M., Takahashi, M., Ono, Y. & Meek, D.W. Centrosomal
849 anchoring of the protein kinase CK1delta mediated by attachment to the
850 large, coiled-coil scaffolding protein CG-NAP/AKAP450. *J Mol Biol* **322**, 785-
851 797 (2002).

- 852 25. Esseltine, J.L. & Scott, J.D. AKAP signaling complexes: pointing towards the
853 next generation of therapeutic targets? *Trends Pharmacol Sci* **34**, 648-655
854 (2013).
- 855 26. Manning, G., Whyte, D.B., Martinez, R., Hunter, T. & Sudarsanam, S. The
856 protein kinase complement of the human genome. *Science* **298**, 1912-1934
857 (2002).
- 858 27. Cummins, T.D. *et al.* FAM83G/PAWS1 controls cytoskeletal dynamics and cell
859 migration through association with the SH3 adaptor CD2AP. *bioRxiv* (2017).
- 860 28. Okamura, H. *et al.* A conserved docking motif for CK1 binding controls the
861 nuclear localization of NFAT1. *Mol Cell Biol* **24**, 4184-4195 (2004).
- 862 29. Kuga, T. *et al.* FAM83H and casein kinase I regulate the organization of the
863 keratin cytoskeleton and formation of desmosomes. *Sci Rep* **6**, 26557 (2016).
- 864 30. Bozatzi, P. *et al.* PAWS1/FAM83G controls Wnt signalling through association
865 with Casein Kinase 1-alpha. *Manuscript being submitted in parallel* (2017).
- 866 31. Barik, S., Taylor, R.E. & Chakrabarti, D. Identification, cloning, and mutational
867 analysis of the casein kinase 1 cDNA of the malaria parasite, Plasmodium
868 falciparum. Stage-specific expression of the gene. *J Biol Chem* **272**, 26132-
869 26138 (1997).
- 870 32. Alexa, A., Varga, J. & Remenyi, A. Scaffolds are 'active' regulators of signaling
871 modules. *FEBS J* **277**, 4376-4382 (2010).
- 872 33. Buday, L. & Tompa, P. Functional classification of scaffold proteins and
873 related molecules. *FEBS J* **277**, 4348-4355 (2010).
- 874 34. Hu, J., Neiswinger, J., Zhang, J., Zhu, H. & Qian, J. Systematic Prediction of
875 Scaffold Proteins Reveals New Design Principles in Scaffold-Mediated Signal
876 Transduction. *PLoS Comput Biol* **11**, e1004508 (2015).
- 877 35. Logue, J.S. & Scott, J.D. Organizing signal transduction through A-kinase
878 anchoring proteins (AKAPs). *FEBS J* **277**, 4370-4375 (2010).
- 879 36. Bayliss, R., Sardon, T., Vernos, I. & Conti, E. Structural basis of Aurora-A
880 activation by TPX2 at the mitotic spindle. *Mol Cell* **12**, 851-862 (2003).
- 881 37. Kuga, T. *et al.* Casein kinase 1 is recruited to nuclear speckles by FAM83H and
882 SON. *Sci Rep* **6**, 34472 (2016).
- 883 38. Badura, L. *et al.* An inhibitor of casein kinase I epsilon induces phase delays in
884 circadian rhythms under free-running and entrained conditions. *J Pharmacol*
885 *Exp Ther* **322**, 730-738 (2007).
- 886 39. Behrend, L. *et al.* IC261, a specific inhibitor of the protein kinases casein
887 kinase 1-delta and -epsilon, triggers the mitotic checkpoint and induces p53-
888 dependent postmitotic effects. *Oncogene* **19**, 5303-5313 (2000).
- 889 40. Chijiwa, T., Hagiwara, M. & Hidaka, H. A newly synthesized selective casein
890 kinase I inhibitor, N-(2-aminoethyl)-5-chloroisoquinoline-8-sulfonamide,
891 and affinity purification of casein kinase I from bovine testis. *J Biol Chem* **264**,
892 4924-4927 (1989).
- 893 41. Rena, G., Bain, J., Elliott, M. & Cohen, P. D4476, a cell-permeant inhibitor of
894 CK1, suppresses the site-specific phosphorylation and nuclear exclusion of
895 FOXO1a. *EMBO Rep* **5**, 60-65 (2004).
- 896 42. Walton, K.M. *et al.* Selective inhibition of casein kinase 1 epsilon minimally
897 alters circadian clock period. *J Pharmacol Exp Ther* **330**, 430-439 (2009).

43. Fulcher, L.J. *et al.* An affinity-directed protein missile system for targeted proteolysis. *Open Biol* **6** (2016).
44. Rojas-Fernandez, A. *et al.* Rapid generation of endogenously driven transcriptional reporters in cells through CRISPR/Cas9. *Sci Rep* **5**, 9811 (2015).
45. Herhaus, L., Al-Salihi, M., Macartney, T., Weidlich, S. & Sapkota, G.P. OTUB1 enhances TGFbeta signalling by inhibiting the ubiquitylation and degradation of active SMAD2/3. *Nat Commun* **4**, 2519 (2013).
46. Bruce, D.L., Macartney, T., Yong, W., Shou, W. & Sapkota, G.P. Protein phosphatase 5 modulates SMAD3 function in the transforming growth factor-beta pathway. *Cell Signal* **24**, 1999-2006 (2012).
47. Herhaus, L. *et al.* Casein kinase 2 (CK2) phosphorylates the deubiquitylase OTUB1 at Ser16 to trigger its nuclear localization. *Sci Signal* **8**, ra35 (2015).
48. Allan, C. *et al.* OMERO: flexible, model-driven data management for experimental biology. *Nat Methods* **9**, 245-253 (2012).
49. Adler, J. & Parmryd, I. Quantifying colocalization by correlation: the Pearson correlation coefficient is superior to the Mander's overlap coefficient. *Cytometry A* **77**, 733-742 (2010).
50. Otsu, N. Threshold Selection Method from Gray-Level Histograms. *Ieee T Syst Man Cyb* **9**, 62-66 (1979).
51. Hastie, C.J., McLauchlan, H.J. & Cohen, P. Assay of protein kinases using radiolabeled ATP: a protocol. *Nat Protoc* **1**, 968-971 (2006).

Figure Legends

Figure 1: Generation of HEK-293 and U2OS cells for tetracycline-inducible expression of FAM83 proteins. **A.** Schematic representation of the human FAM83 family of proteins and the conserved *DUF1669* domain of unknown function that characterises them. **B.** A single copy of each FAM83A-H gene each tagged with GFP at the N-terminus was stably inserted downstream of a tetracycline-inducible promoter in Flp-In T-Rex HEK-293 cells. Cells were treated with 20 ng/ml doxycycline and lysed at the indicated times after treatment. Extracts (10 µg protein) were resolved by SDS-PAGE and subjected to immunoblotting with the indicated antibodies. **C.** As in B, except that Flp-In T-Rex U2OS cells were used and the GFP tag was inserted at the C-terminus of the FAM83 genes. We were unable to detect FAM83B-GFP in U2OS cells.

Figure 2: FAM83 proteins interact with CK1 isoforms. **A.** Mass fingerprinting of protein interactors of N-terminal (HEK-293 cells) or C-terminal (U2OS cells) GFP-tagged FAM83A-H proteins (fig. S2, A and B) identified one or more CK1 α , α -like, δ and ϵ isoforms. Included in the tables are values for the top 3 precursor ion intensities of the indicated CK1 isoforms identified in each GFP-FAM83A-H (HEK-293) and FAM83A-H-GFP (U2OS), and control GFP pull-down obtained using Scaffold Q/Q+S V4.4.6 (HEK-293 cells) and V4.3 (U2OS cells) analysis of the LC-MS-MS data. Note: FAM83B-GFP did not express in U2OS cells. **B.** IPs of GFP control or GFP-FAM83A-H proteins expressed in Flp-In T-Rex HEK-293 cells, resolved by SDS-PAGE and transferred to PVDF membranes, were subjected to immunoblotting with antibodies against the indicated CK1 isoforms and other interacting proteins. **C.** Wild-type (WT) or GFP-FAM83B knockin (^{GFP/GFP}FAM83B) HaCaT cells were lysed and extracts (5 mg protein) subjected to IP with GFP-trap beads. IPs, Input extracts (20 μ g), and post-IP flowthrough extracts (20 μ g protein), were resolved by SDS-PAGE and transferred to PVDF membranes, before being subjected to immunoblotting with antibodies against the indicated CK1 isoforms and GAPDH. **D.** As in C., except that wild type (WT) U2OS and FAM83G-GFP knockin (FAM83G^{GFP/GFP}) U2OS cells were employed. **E.** U2OS extracts (1 mg protein) were subjected to IPs using either pre-immune IgG or anti-CK1 α antibody (10 μ g) coupled to Protein-G sepharose beads (10 μ l). Input extracts (20 μ g) and IPs were resolved by SDS-PAGE, transferred to PVDF membranes and subjected to immunoblotting with antibodies against the indicated FAM83 proteins and GAPDH.

Figure 3: The DUF1669 domain of FAM83 members is sufficient in mediating the interaction with CK1 isoforms. **A.** The indicated fragments of Myc-tagged FAM83G were co-expressed with HA-CK1 α in FAM83G^{-/-} U2OS cells for 48 h. Anti-HA IPs or extracts were subjected to immunoblotting with anti-myc and anti-HA antibodies as indicated. **B.** The FAM83A PLD-like domain forms a direct interaction with the CK1 ϵ kinase domain. Ni-sepharose agarose resin was loaded with 6xHis-FAM83A(122-304) fragment and used to pull down CK1 ϵ kinase domain (a.a. 1-294). Resin was washed twice with buffer containing 5 mM imidazole before elution with 250 mM imidazole. The input, flow through (FT), washes (W1 and W2) and elution (E) were analysed by SDS-PAGE gel stained with Coomassie blue. **C.** Control Flag-vector or the indicated FLAG-tagged FAM83G mutants were overexpressed in FAM83G^{-/-} U2OS cells. Anti-FLAG IPs

or extracts were subjected to immunoblotting with anti-FLAG and anti-CK1 α antibodies as indicated. **D.** WT and F/A & D/A mutants of GFP-FAM83E-H were transiently expressed in U2OS cells. Input extracts and GFP-trap IPs were resolved by SDS-PAGE, transferred to PVDF membranes and probed using antibodies against GFP, CK1 α and CK1 ϵ as indicated.

Figure 4: FAM83 proteins and mCherry-CK1 α co-localize in cells. U2OS cells stably integrated with Tet-inducible expression of GFP-FAM83A-H were transfected with mCherry-CK1 α . GFP-FAM83A-H expression was induced with doxycycline for 24 h, prior to fixing cells in PFA for fluorescence microscopy. Images were taken using a Nikon TiS inverted microscope. Images were processed using NIS Elements (Nikon) and Adobe Photoshop using identical parameters across all the images. Images from one field of view representative of three biological replicates are included. The number of cells across biological replicates which displayed identical staining patterns as the representative image were documented for each experiment: GFP-FAM83A (n=50); GFP-FAM83B (n=31); GFP-FAM83C (n=37); GFP-FAM83D (n=32); GFP-FAM83E (n=55); GFP-FAM83F (n=44); GFP-FAM83G (n=43); GFP-FAM83H (n=32). Fluorescence images for GFP-alone and mCherry-CK1 α alone expressing cells are included in Supplementary Figure 6 (fig. S6).

Figure 5: FAM83 proteins and endogenous CK1 α co-localize in cells.

U2OS cells stably integrated with Tet-inducible expression of GFP-alone (negative control) or GFP-FAM83B, F or H were treated with doxycycline for 16 h, prior to fixing cells for fluorescence microscopy. Following fixation in PFA, cells were stained with anti-CK1 α antibody for visualising endogenous CK1 α as indicated. Images were taken using a DeltaVision widefield fluorescence microscope and deconvolved using SoftWorx. Images from one field of view representative of three biological replicates are included. The number of cells across biological replicates which displayed identical staining patterns as the representative image were documented for each experiment: GFP-FAM83B (n=56); GFP-FAM83F (n=60); GFP-FAM83H (n=48); GFP only (n=38); CK1 α only (n=82). Scale bars represent 20 μ m.

Figure 6: Selectivity of association between FAM83 proteins and specific CK1 isoforms persists in cells. A. U2OS cells stably integrated with Tet-inducible

expression of GFP-FAM83F or GFP-FAM83H were transfected with either mCherry-CK1 α or mCherry-CK1 ϵ . GFP-FAM83F and GFP-FAM83H expression was induced with doxycycline for 24 h, prior to fixing cells in PFA for fluorescence microscopy. Images were taken using a DeltaVision widefield fluorescence microscope and deconvolved using SoftWorx. Images from one field of view representative of three biological replicates are included. The number of cells across biological replicates which displayed identical staining patterns as the representative image were documented for each experiment: GFP-FAM83F + mCherry-CK1 α (n=44); GFP-FAM83F + mCherry-CK1 ϵ (n=40); GFP-FAM83H + mCherry-CK1 α (n=32); GFP-FAM83H + mCherry-CK1 ϵ (n=40). Scale bars represent 20 μ m. **B.** U2OS cells stably integrated with Tet-inducible expression of GFP-FAM83F or H were induced with doxycycline for 16 h, prior to fixing cells for fluorescence microscopy. Cells were either left unstained, or stained with anti-CK1 α or CK1 ϵ to visualise endogenous CK1 α and CK1 ϵ respectively. Untransfected cells stained with anti-CK1 α or CK1 ϵ were used as negative controls. Images were taken using a DeltaVision widefield fluorescence microscope and deconvolved using SoftWorx. Images from one field of view representative of three biological replicates are included. The number of cells across biological replicates which displayed identical staining patterns as the representative image were documented for each experiment: GFP-FAM83F+CK1 α (n=60); GFP-FAM83F+CK1 ϵ (n=43); GFP-FAM83H+CK1 α (n=48); GFP-FAM83H+CK1 ϵ (n=35); CK1 α only (n=82); CK1 ϵ only (n=27). Scale bars represent 20 μ m.

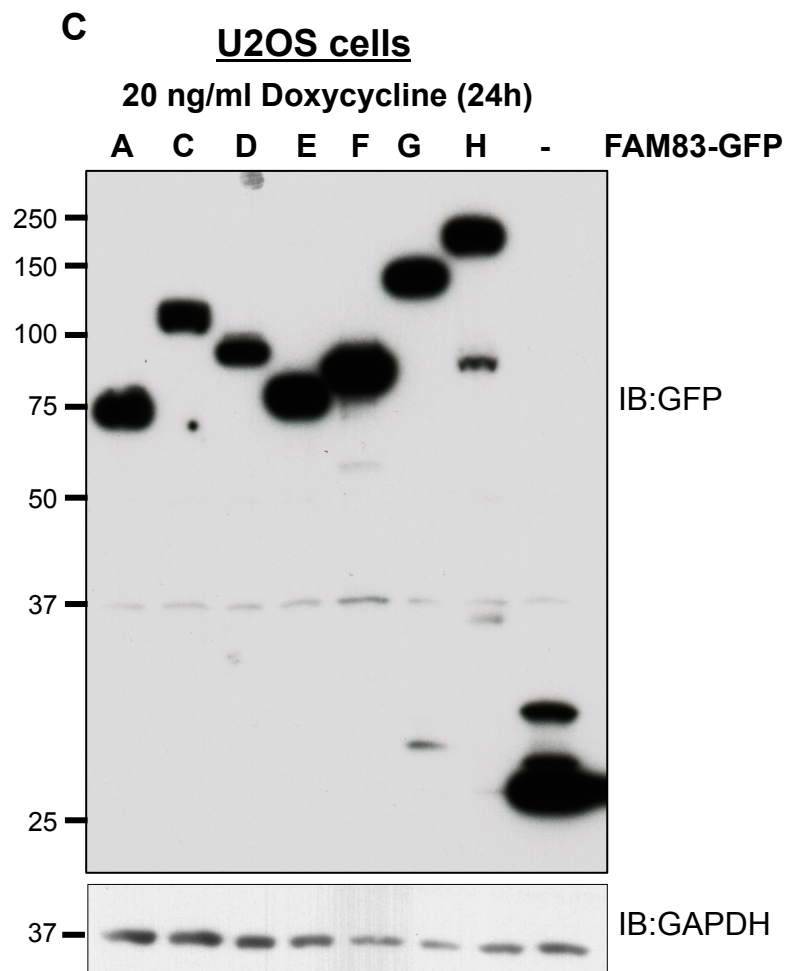
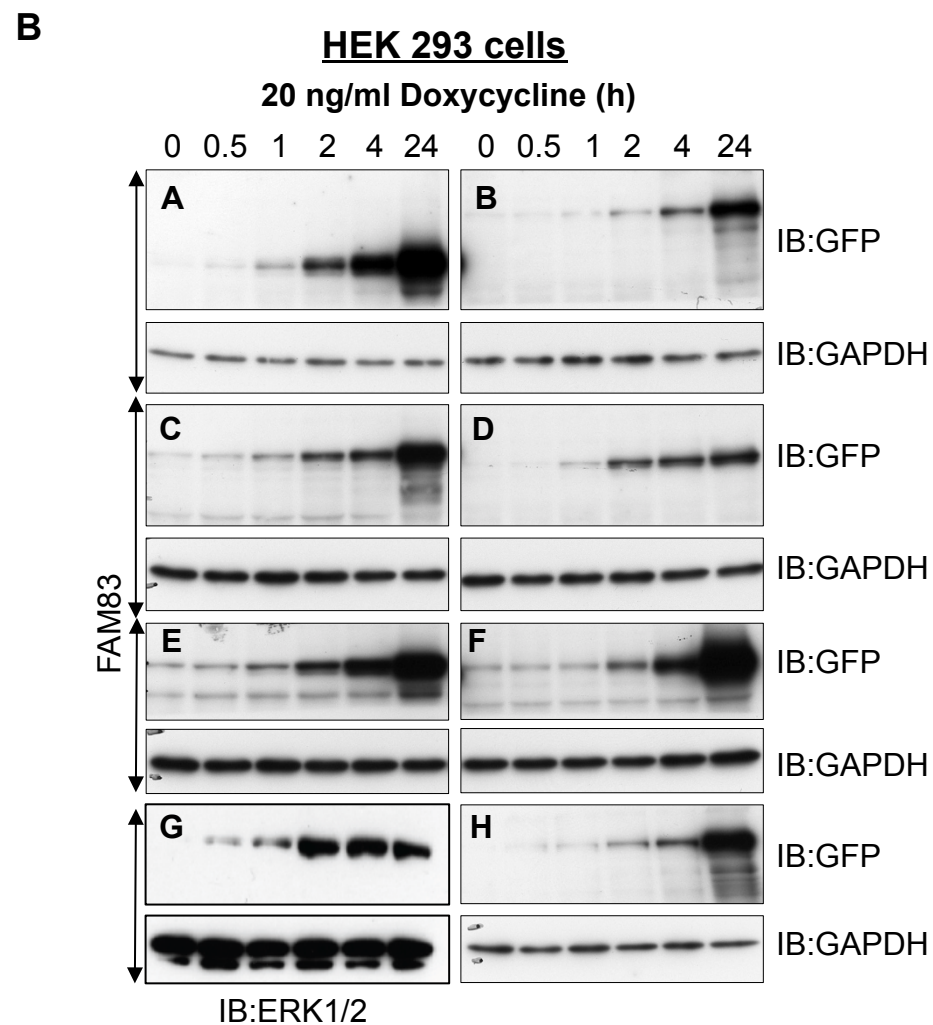
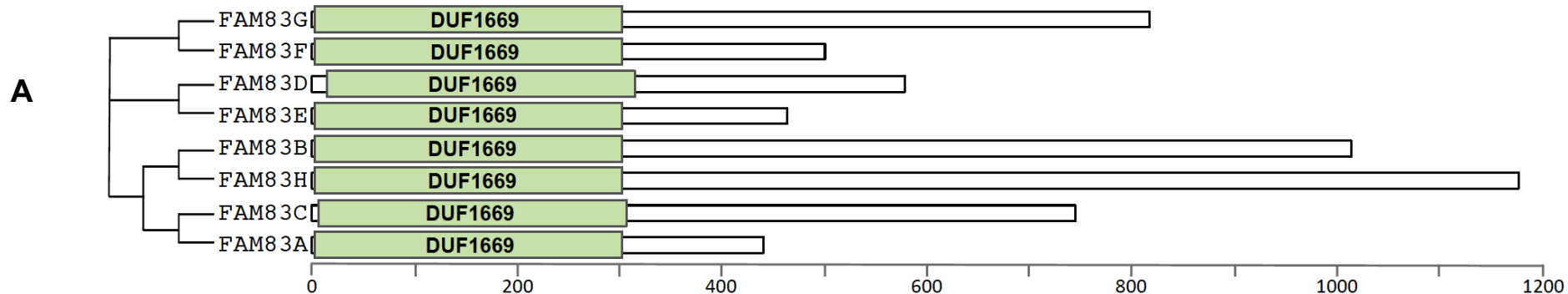
Figure 7: The subcellular localization of FAM83C is determined by its association with CK1. **A.** U2OS cells were co-transfected with plasmids encoding either GFP-control, wild-type GFP-FAM83C (WT), GFP-FAM83C-F293A (F/A) or GFP-FAM83C-D259A (D/A) and HA-CK1 α . Untransfected and HA-CK1 α only-transfected cells were included as controls. Input extracts (20 μ g) or GFP-trap IPs were resolved by SDS-PAGE, transferred to PVDF membranes and subjected to immunoblotting with antibodies against GFP and CK1 α . **B.** U2OS cells were transfected with plasmids encoding either wild-type GFP-FAM83C, GFP-FAM83C-F293A or GFP-FAM83C-D259A together with mCherry-CK1 α as indicated. Representative images from cells expressing GFP-FAM83C or mCherry-CK1 α alone are also included. 24 h-post transfection cells were fixed with PFA and processed for fluorescence microscopy. Images were taken

using a DeltaVision widefield fluorescence microscope and deconvolved using SoftWorx. Images from one field of view representative of three biological replicates are included. The number of cells across biological replicates which displayed identical staining patterns as the representative image were documented for each experiment: GFP-FAM83C only (n=46); GFP-FAM83C + mCherry-CK1 α (n=44); GFP-FAM83C(F293A) + mCherry-CK1 α (n=41); GFP-FAM83C(D259A) + mCherry-CK1 α (n=43); mCherry-CK1 α only (n=45). Scale bars represent 20 μ m.

Figure 8: FAM83H co-localizes with, and in part determines the subcellular localization of, endogenous CK1 α . **A.** FAM83H^{-/-} U2OS cells were transfected with rescue (Res) vectors encoding GFP-FAM83H, GFP-FAM83H-D236A, GFP-FAM83H-F270A mutants or not transfected (FAM83H KO). Cells were fixed in methanol and stained with anti-CK1 α primary antibody followed by anti-goat AlexaFluor-594 conjugated secondary antibodies. DNA was stained with DAPI. Representative images from one field of view are included. Scale bars represent 10 μ m. **B.** The boxplot shows the range, mean, lower and upper quartile of the Pearson's correlation coefficients of GFP-FAM83H and endogenous CK1 α intensities within above-background pixels in the cytoplasm. Data was obtained from three separate experiments. The mean Pearson's correlation coefficients for different rescue mutants are as follows: FAM83H^{WT}=0.7523, FAM83H^{D236A}=0.09972 and FAM83H^{F270A}=0.001504. **C.** Analysis of protein expression of rescue constructs transfected in FAM83H^{-/-} U2OS cells in comparison to WT cells as indicated by Western blotting.

Figure 9: Dissecting the links between intrinsic CK1 kinase activity and the FAM83:CK1 interaction. **A.** An in vitro kinase assay was set up using 200 ng of GST-CK1 α , 2 μ g of substrate (GST-FAM83A, C, D, E, F, or H, MBP-FAM83B, or GST-FAM83G-6XHis) and [γ -³²P]-ATP (~500 cpm/pmol). After reactions were stopped, samples were resolved by SDS-PAGE and the gel was stained with Instant blue, dried and subjected to ³²P autoradiography for the indicated times. **B.** An in vitro kinase assay was set up with 50 ng of GST-CK1 α and increasing amounts of CK1tide as indicated. The effects of the addition of equimolar amounts of WT GST-FAM83G-6xHis or CK1 interaction-deficient GST-FAM83G^{F296A/F300A} (FF/AA) mutant on intrinsic CK1 α activity were evaluated. Data points represent the average from 9 replicates. Error bars

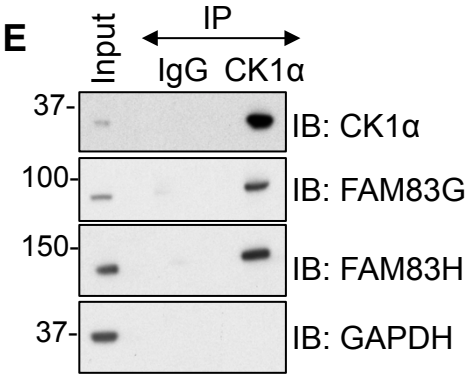
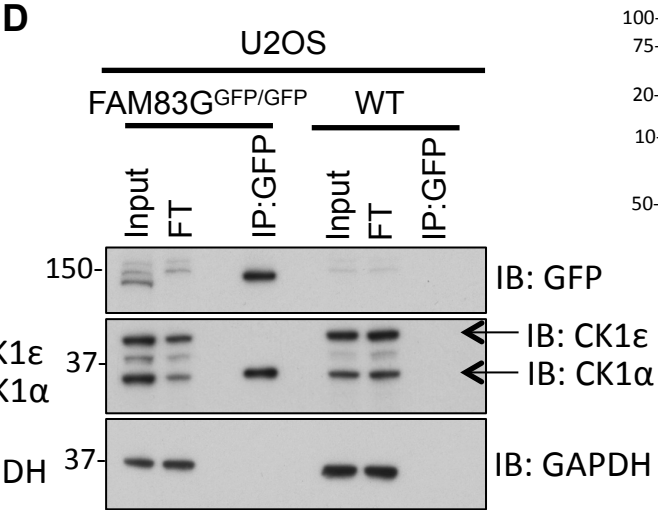
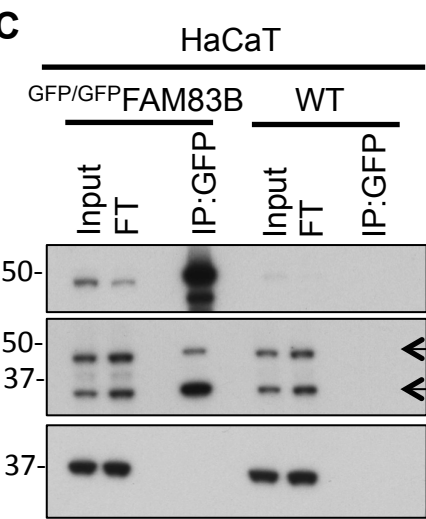
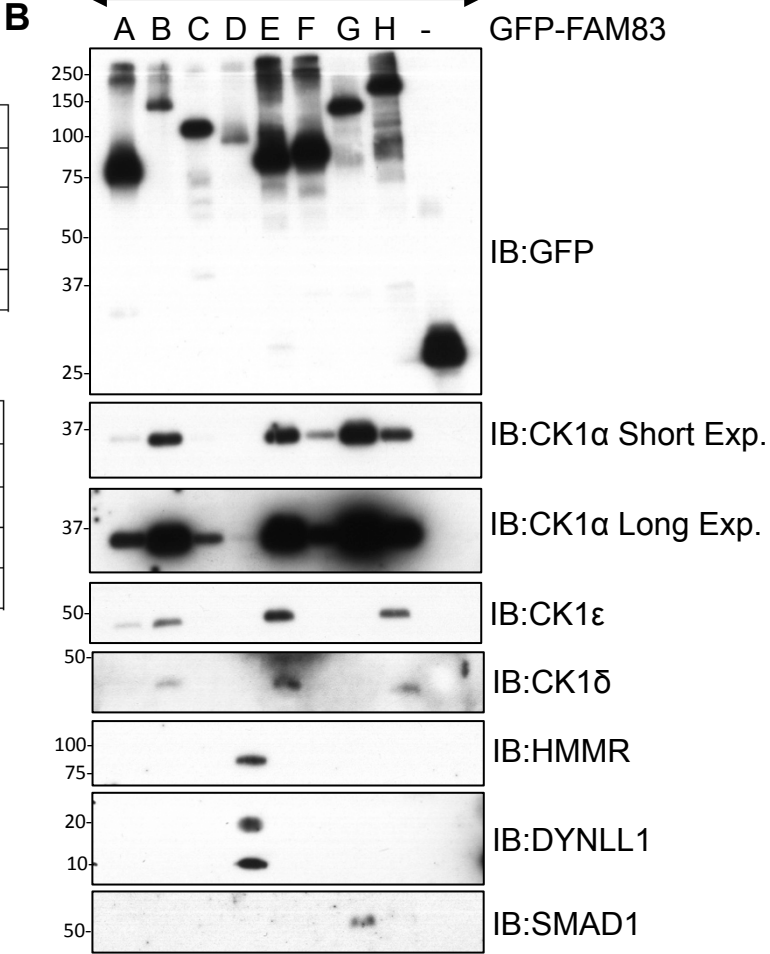
1072 represent SEM. **C.** U2OS cells were transiently co-transfected with GFP-FAM83E-H and
1073 either mCherry-tagged wild-type (WT) CK1 α or a catalytically inactive (kinase dead
1074 (KD)) mutant (CK1 α^{N141A}) for 24 h. Following incubation, cells were lysed and extracts
1075 subjected to GFP-trap IPs. Input and IP samples were resolved by SDS-PAGE,
1076 transferred onto PVDF membranes, and immunoblotted with the indicated antibodies.

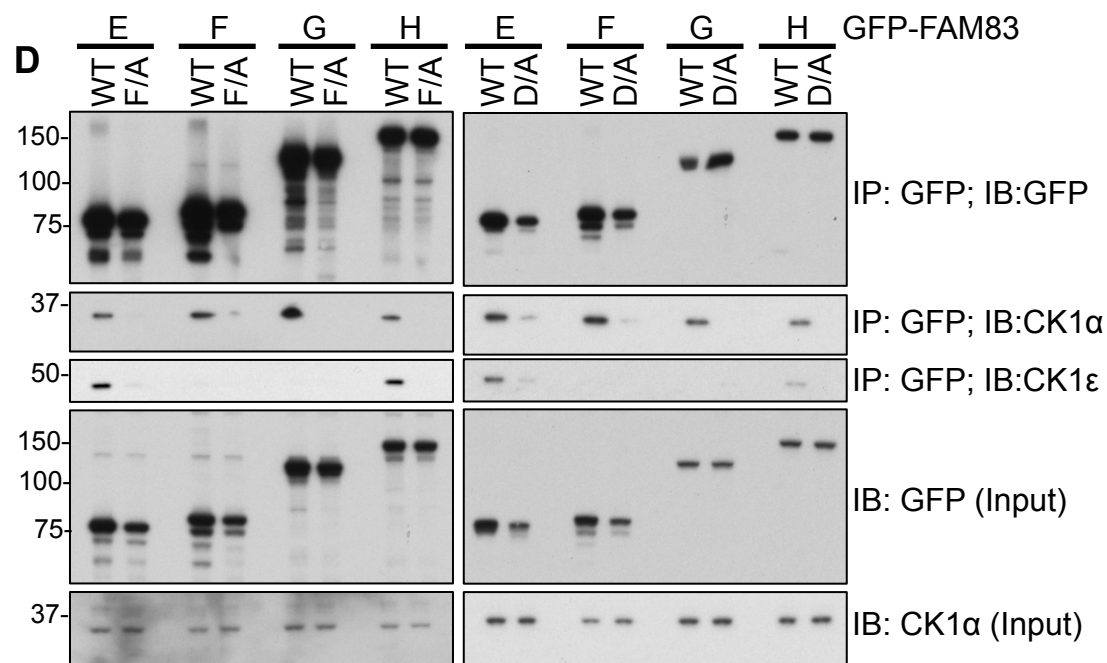
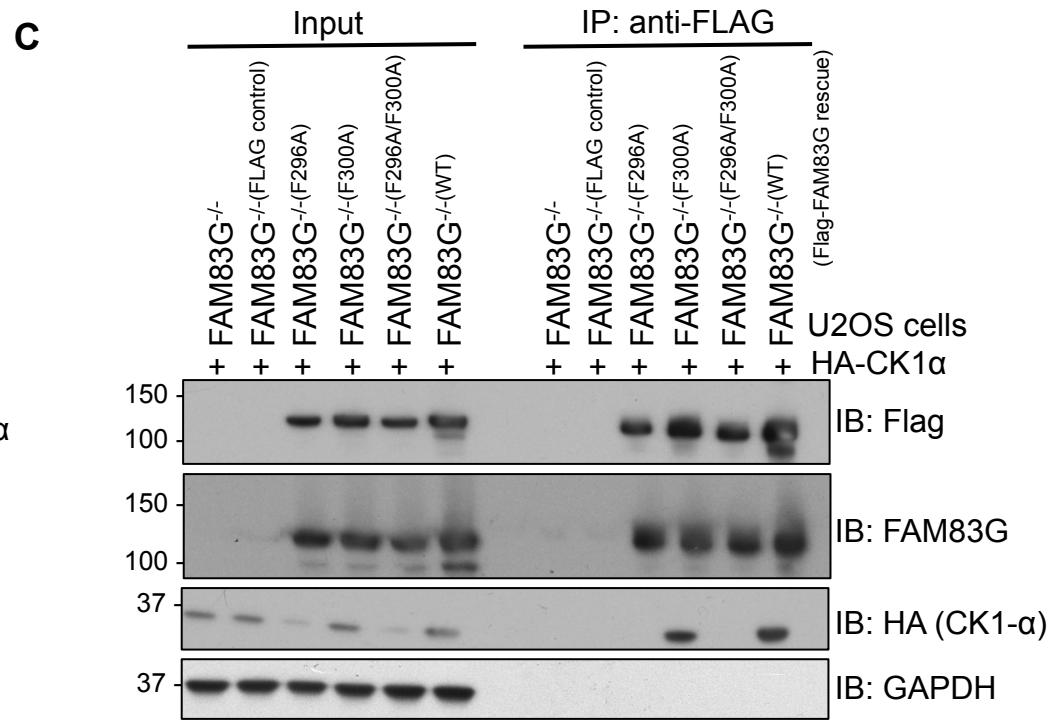
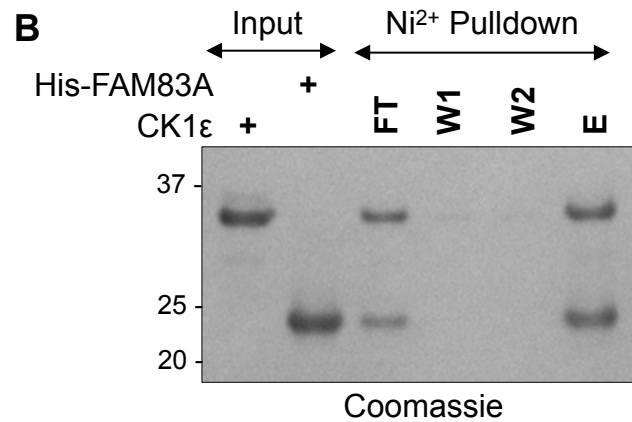
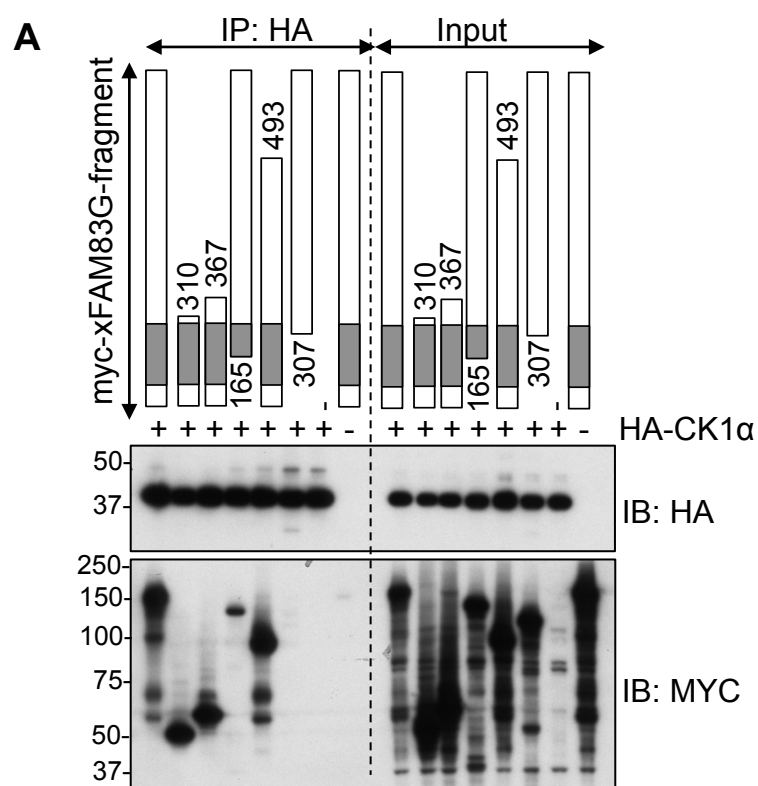


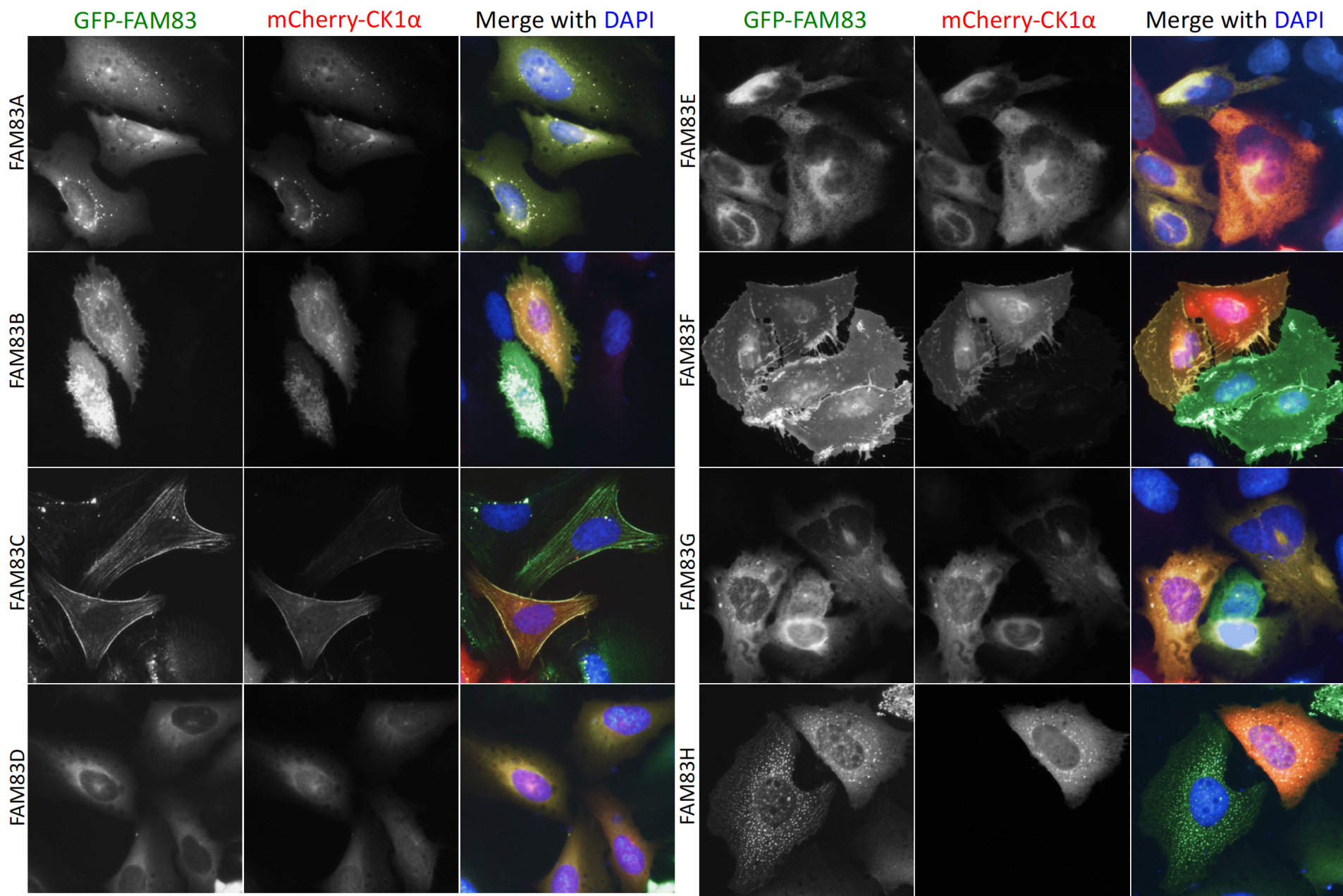
A CK1 isoforms identified by mass-spectrometry in FAM83 IPs

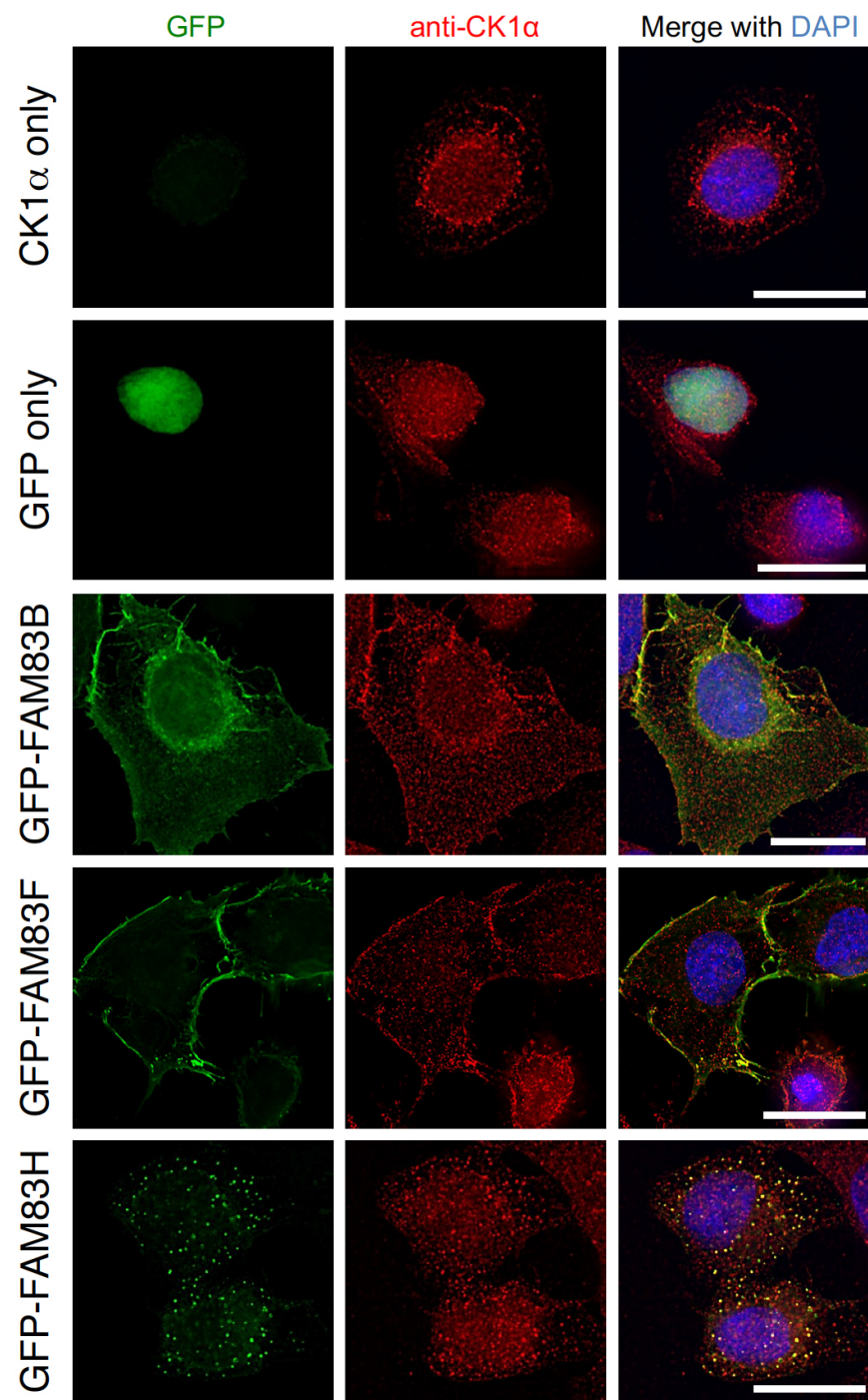
HEK293									
Top 3 precursor ion intensities (x 10 ⁷)									
GFP-FAM83	A	B	C	D	E	F	G	H	GFP
CK1 α	185	828	211	99	662	283	1380	144	10
CK1αL	143	787	176	76	501	232	1060	118	8
CK1δ	127	412	46	7	381	5	16	117	8
CK1ε	127	412	46	8	389	5	19	118	9

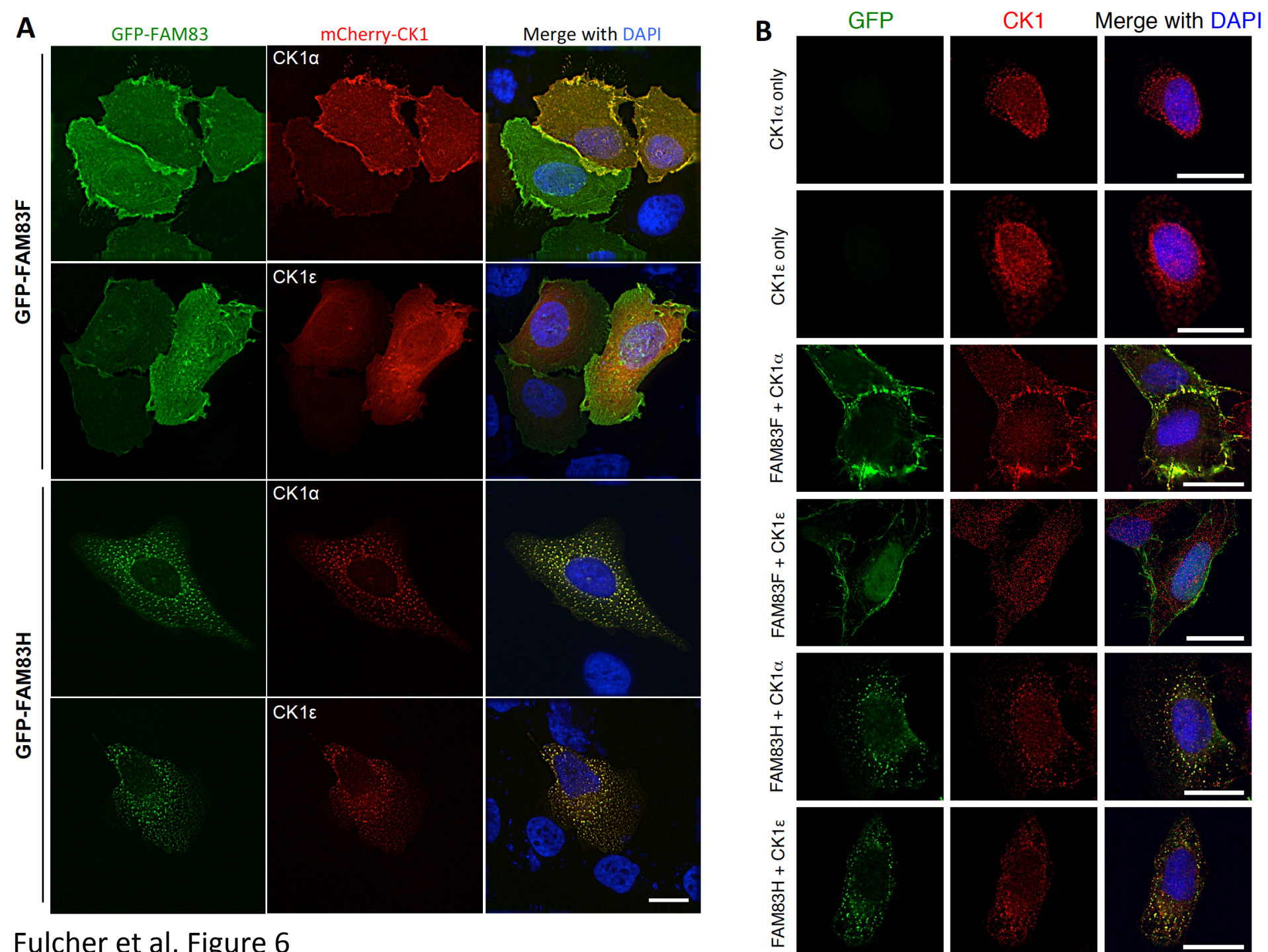
U2OS									
Top 3 precursor ion intensities (x 10 ⁷)									
FAM83-GFP	A	B	C	D	E	F	G	H	GFP
CK1α	101	N/A	36	84	709	902	905	234	1
CK1αL	100	N/A	0	0	668	833	817	0	0
CK1δ	78	N/A	18	13	468	4	9	198	1
CK1ε	99	N/A	28	19	599	5	11	198	2

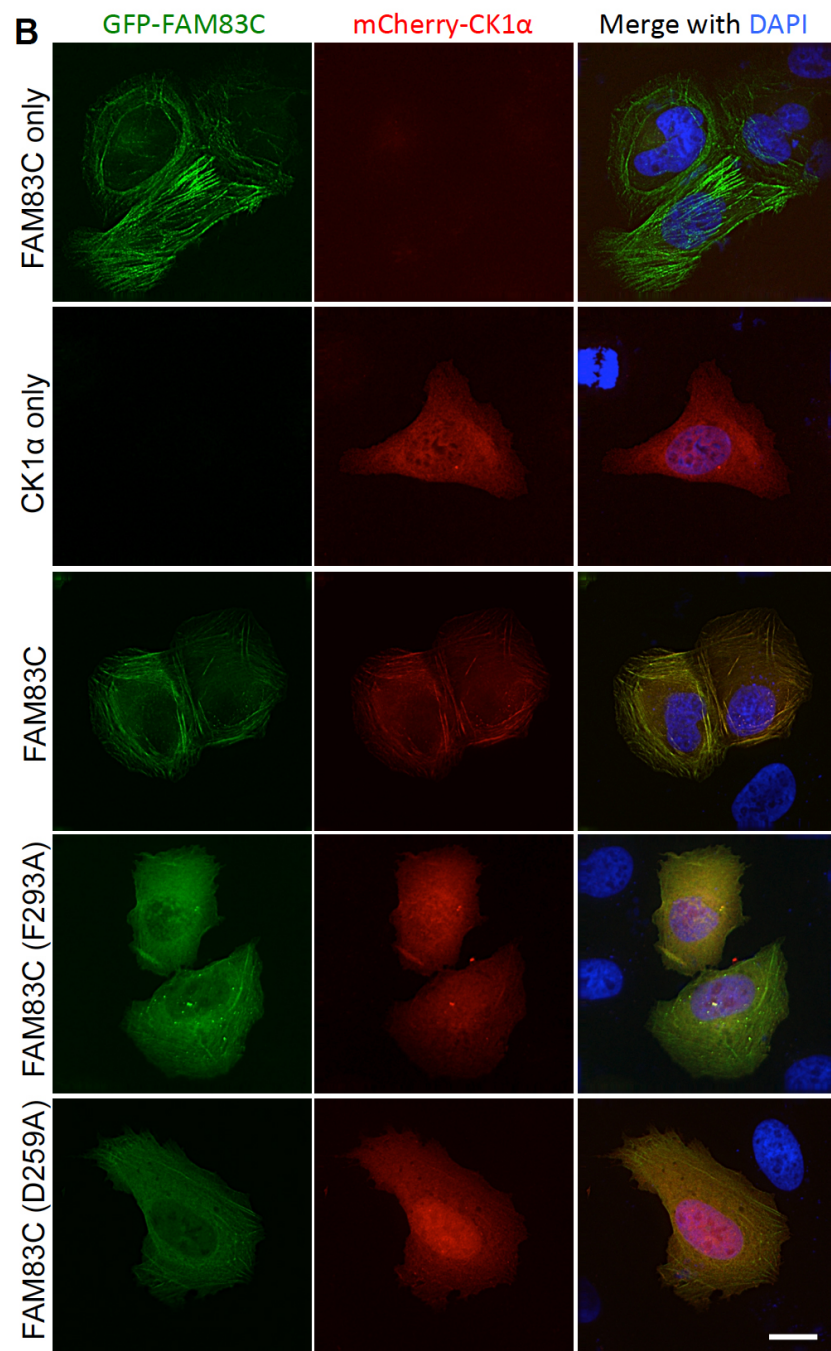
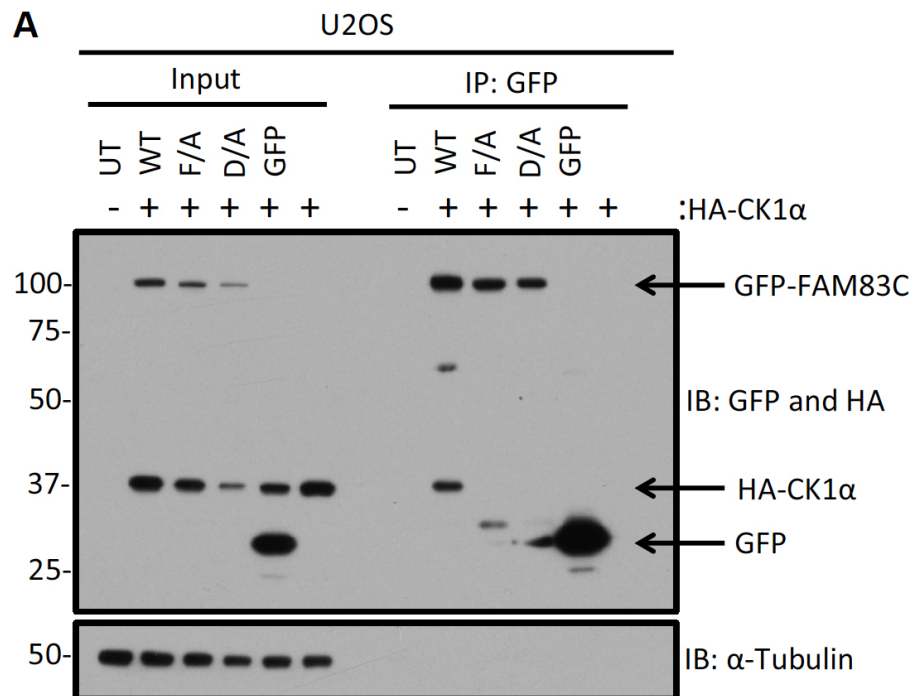










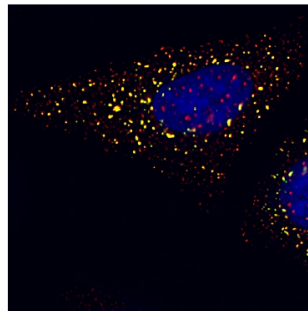
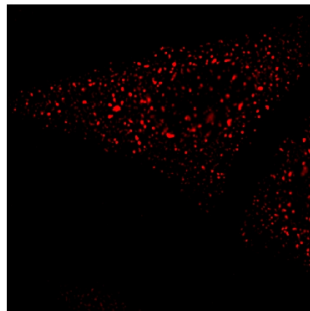
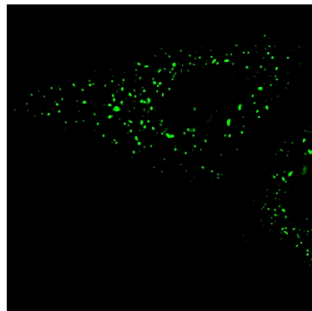
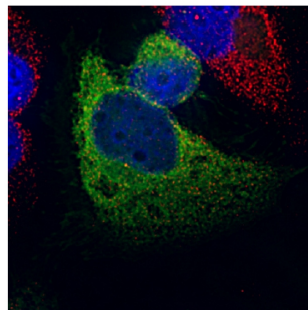
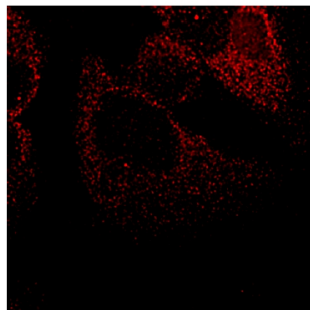
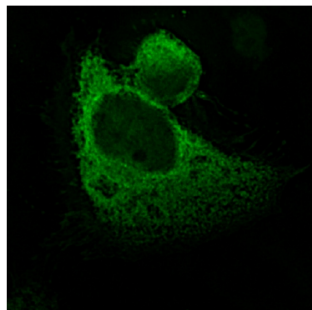
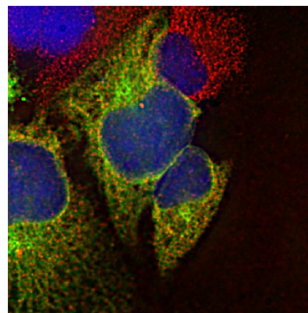
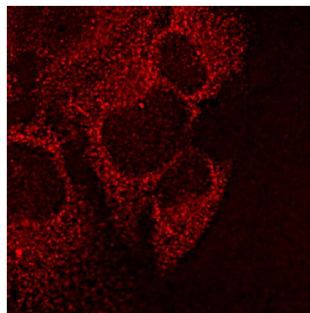
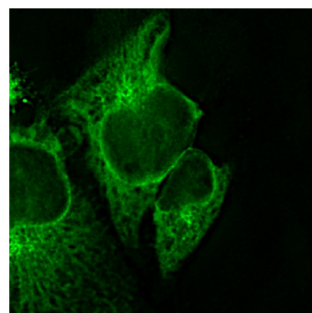


A

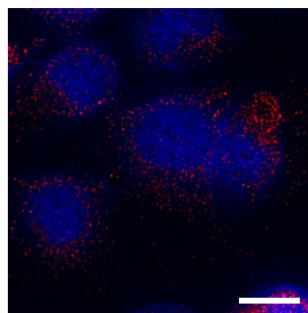
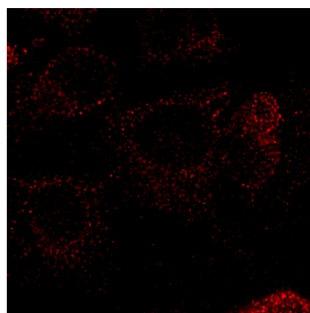
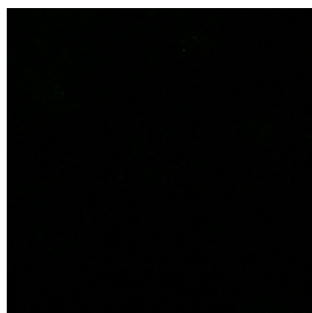
GFP-FAM83H

Endogenous CK1 α

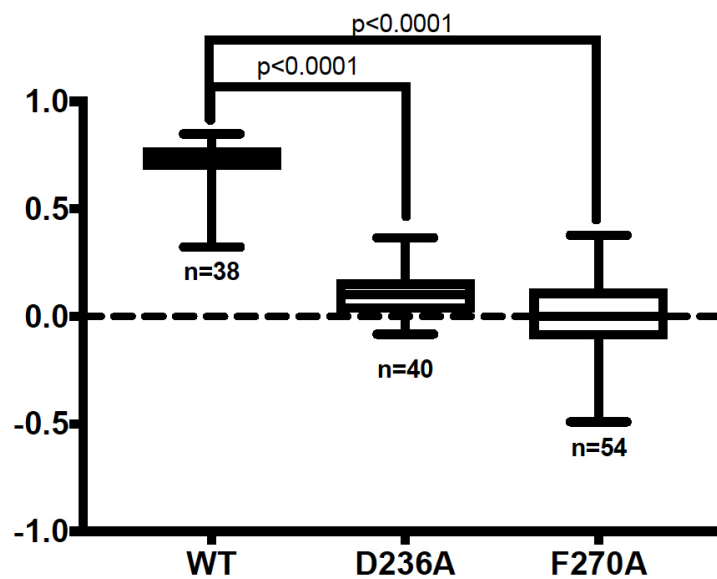
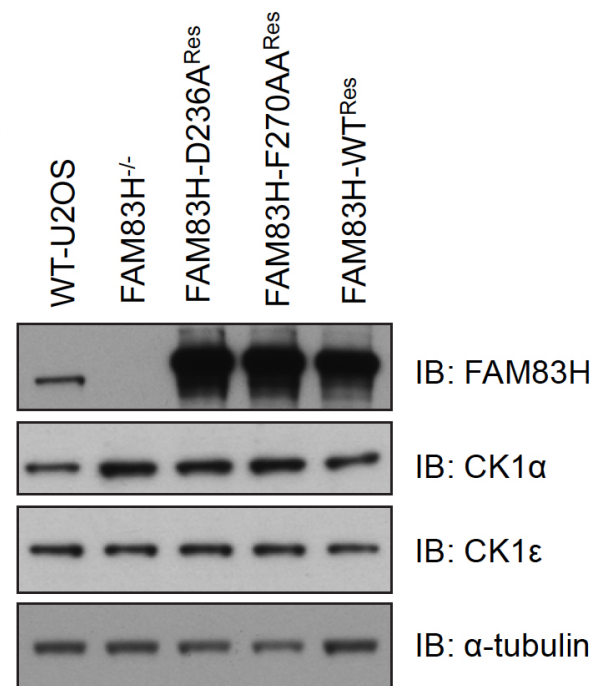
Merge with DAPI

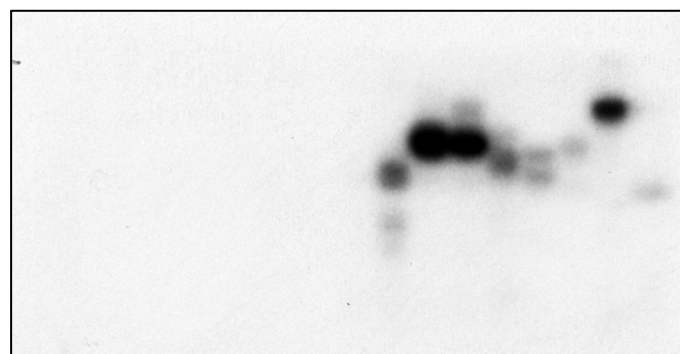
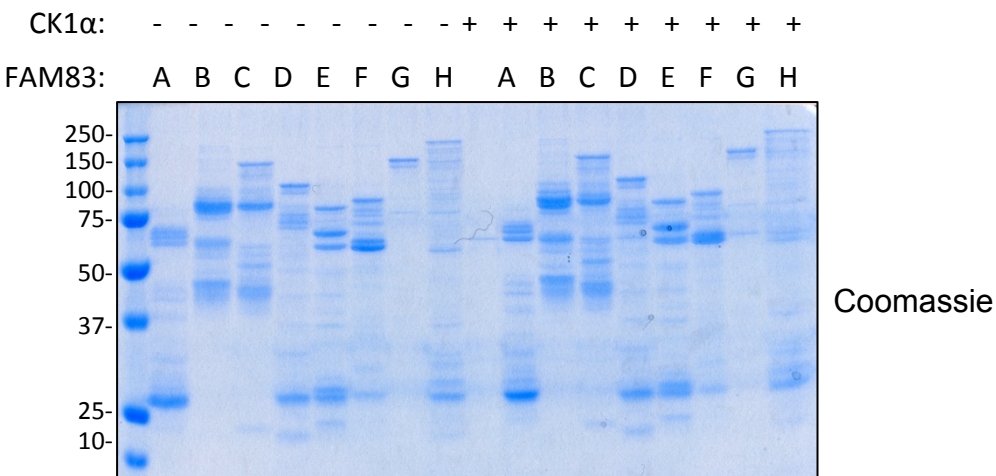
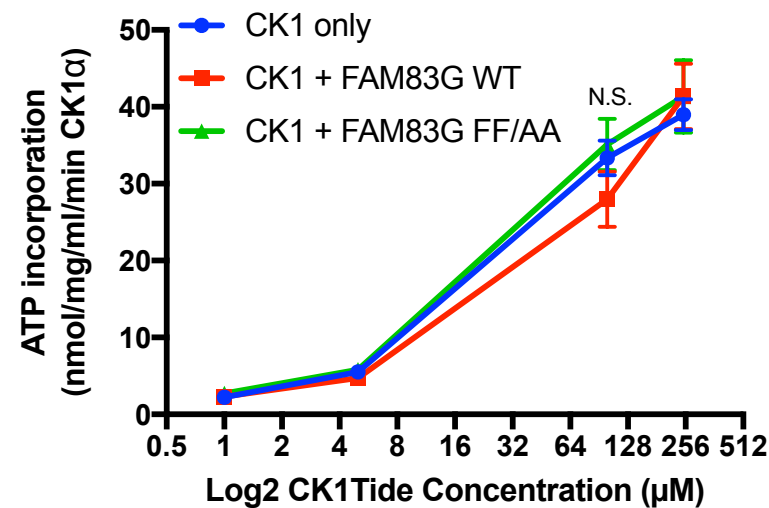
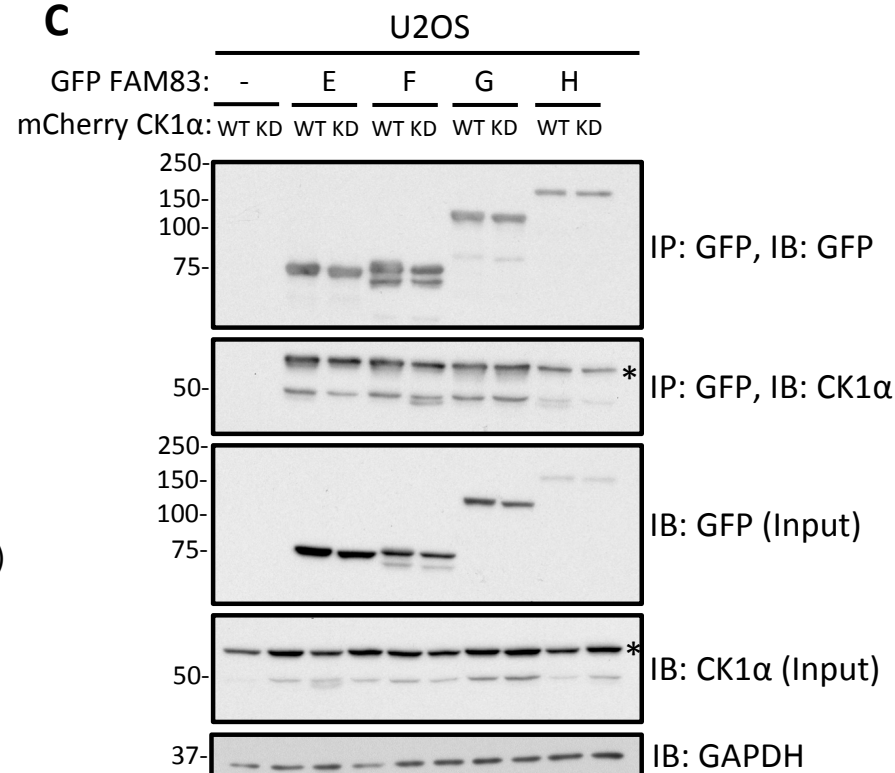
FAM83H-WT^{Res}FAM83H-D236A^{Res}FAM83H-F270A^{Res}

FAM83H-KO

**B**

Pearson's correlation coefficient

**C**

A**B****C**

The FAM83 family of proteins are anchors for Casein Kinase 1 isoforms through the *DUF1669* domain

One sentence summary: The FAM83 proteins serve as subcellular anchors for CK1 isoforms to streamline CK1 signalling.

Luke J Fulcher¹, Polyxeni Bozatzki¹, Theresa Tachie-Menson¹, Kevin Z L Wu¹, Timothy D Cummins¹, Joshua C Bufton³, Daniel M Pinkas³, Karen Dunbar¹, Sabin Shrestha¹, Nicola T Wood¹, Simone Weidlich¹, Thomas J Macartney¹, Joby Varghese¹, Robert Gourlay¹, David G Campbell¹, Kevin S Dingwell², James C Smith², Alex N Bullock³ and Gopal P Sapkota^{1*}

¹Medical Research Council Protein Phosphorylation and Ubiquitylation Unit, Dundee, Scotland, UK, ²The Francis Crick Institute, London, UK, ³Structural Genomics Consortium, University of Oxford, Oxford, UK.

*Address correspondence to g.sapkota@dundee.ac.uk

The PDF file includes:

Fig. S1: Sequence alignment of the *DUF1669* domain of the FAM83 proteins.

Fig. S2: Coomassie images of GFP-trap IPs of FAM83A-H proteins used to identify interacting partners by mass spectrometry

Fig. S3: Immunoblots of input controls for Figure 2

Fig. S4: PAWS1 interacts with CK1 α , but not CK1 γ or TTBK1

Fig. S5: CK1-specificity switch with *DUF1669* chimera

Fig. S6: Fluorescence images of GFP controls

Fig. S7: FAM83H co-localizes with, and in part determines the subcellular localization of, endogenous CK1 ϵ

Fig. S8: Validation of anti-CK1 α and ϵ antibodies for IF applications

Supplementary Method: Supplemental Macro for ImageJ added to quantitate co-localization in cells.

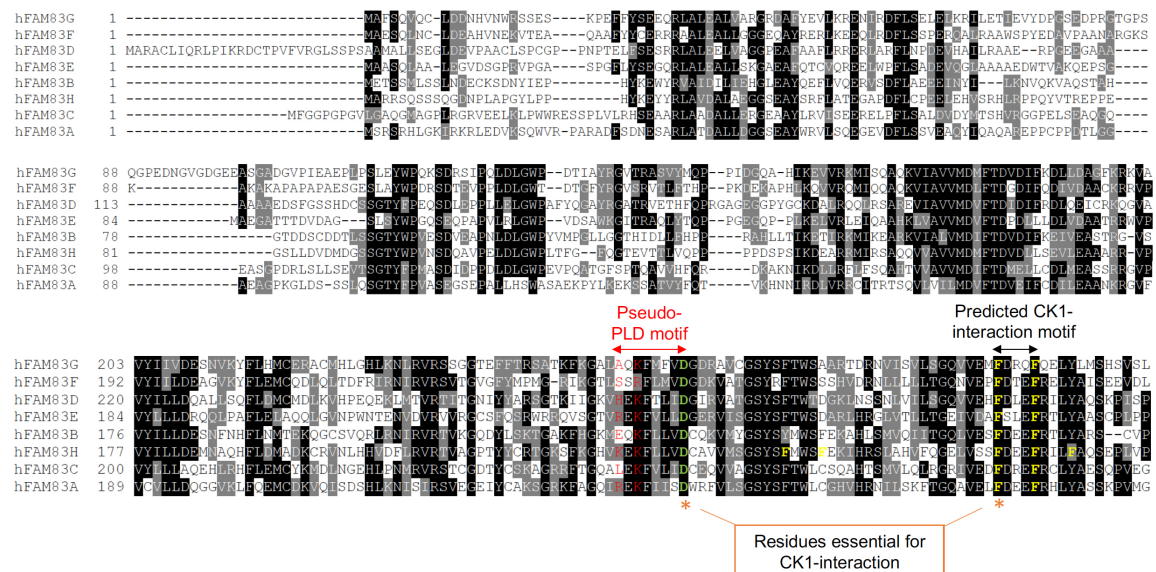


Fig. S1: Sequence alignment of the *DUF1669* domain of the FAM83 proteins. A. Full sequence alignment of the *DUF1669* domain indicating the putative pseudo-PLD catalytic motif, the location of predicted CK1-interaction FXXXF motifs (F in yellow) and the location of two residues essential for CK1-interaction.

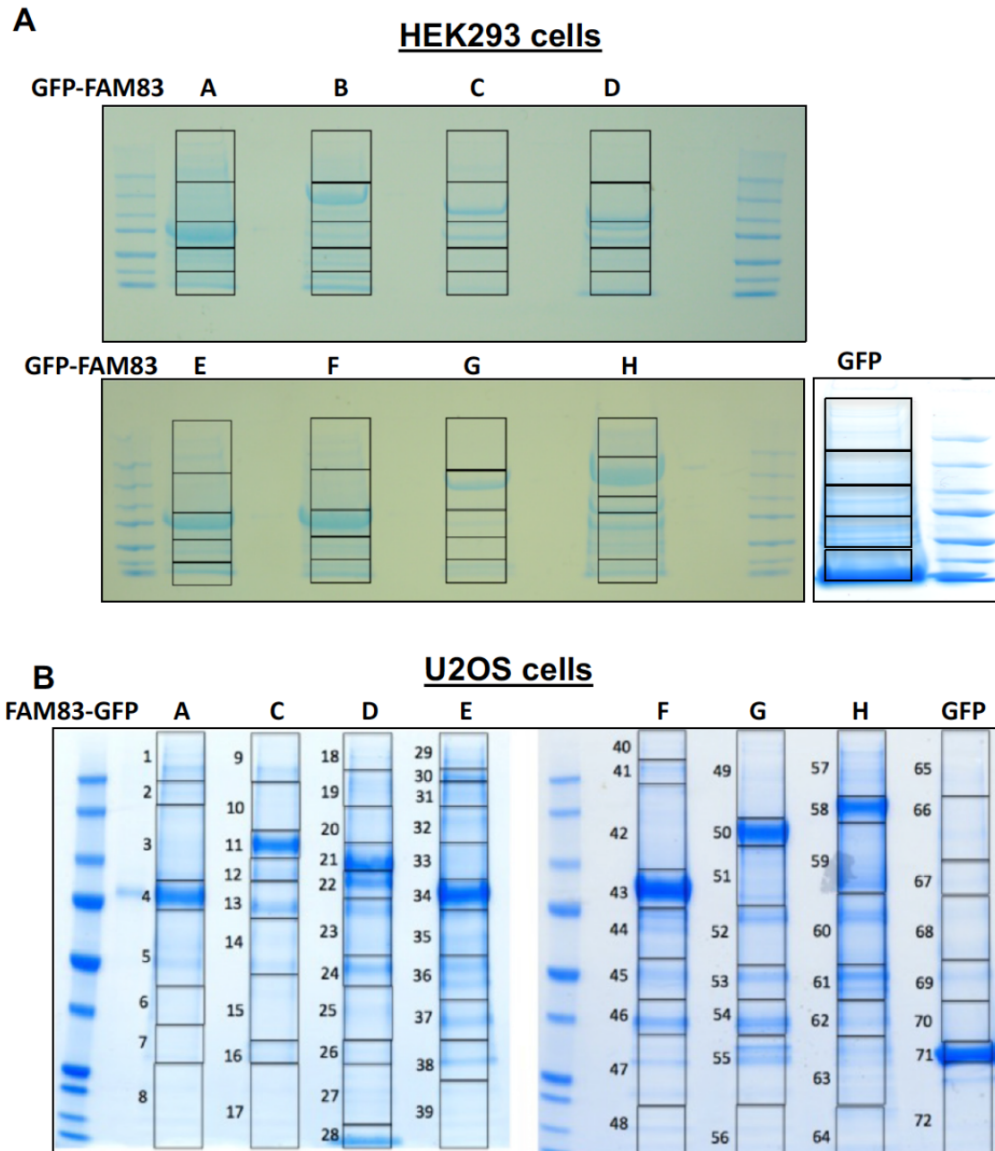


Fig. S2: Coomassie images of GFP-trap IPs of FAM83A-H proteins used to identify interacting partners by mass spectrometry. A. Extracts from doxycycline-treated (20 ng/ml; 24 h) Flp-In T-Rex HEK-293 cells integrated with isogenic copy each of N-terminally GFP-tagged FAM83A-H or GFP alone were subjected to GFP-trap IPs and resolved by SDS-PAGE. The gels were Coomassie stained and imaged. The boxed regions in each lane represent the approximate excisions made in order to perform in-gel trypsin digestion and process the samples for protein identification by mass spectrometry. **B.** As in A, except that extracts from Flp-In T-Rex U2OS cells integrated with isogenic copy each of C-terminally GFP-tagged FAM83A, FAM83C-H or GFP alone were used.

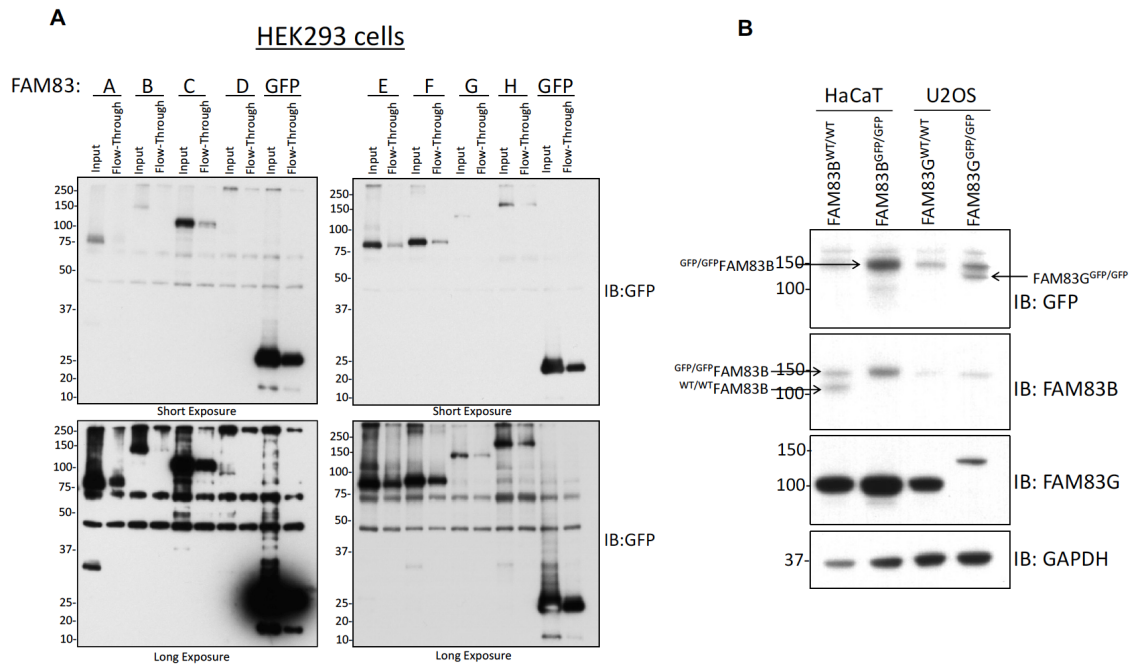


Fig. S3: Immunoblots of input controls for Figure 2. A. Input extracts and post GFP-IP flowthrough extracts (both 20 μ g protein) were resolved by SDS-PAGE, transferred to PVDF membranes and subjected to Western blotting with anti-GFP antibodies to probe for expression of GFP-FAM83A-H proteins as well as the efficiency of GFP-IP. Low and high exposure images are included. **B.** Endogenous FAM83B and FAM83G genes were modified using CRISPR/Cas9 genome editing to insert GFP tags at the N- or C-terminus of the gene respectively. Input extracts were resolved by SDS-PAGE, transferred to PVDF membranes and subjected to immunoblotting using the indicated antibodies.

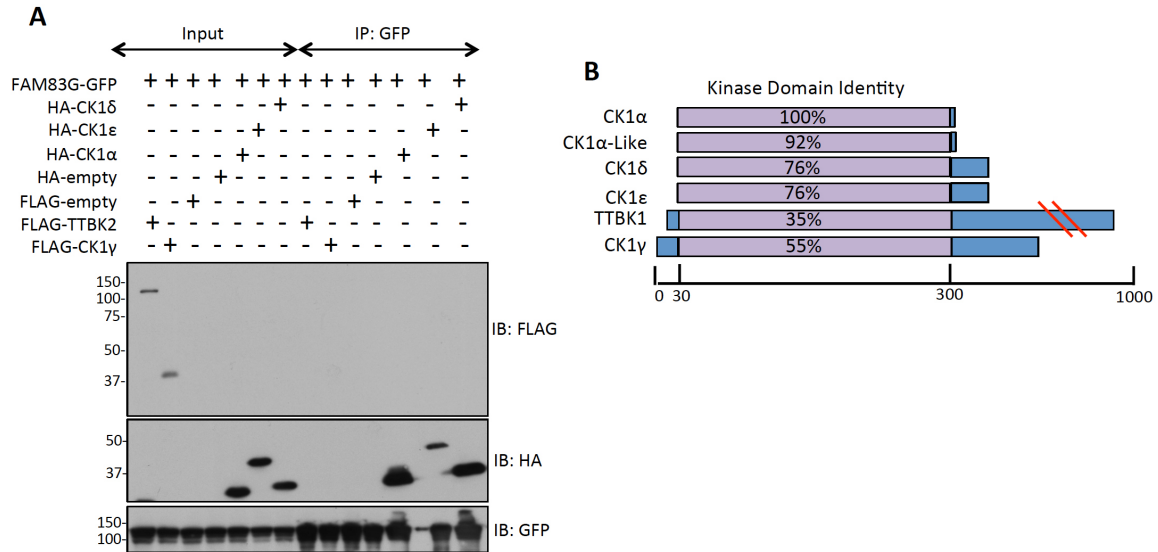


Fig. S4: FAM83G interacts with CK1 α , but not CK1 γ or TTBK1. The indicated FLAG- or HA-tagged CK1 family isoforms were co-expressed with FAM83G-GFP in U2OS cells. Input extracts and GFP-IPs were resolved by SDS-PAGE, transferred to PVDF membranes and subjected to immunoblotting using the indicated antibodies. **B.** Schematic highlighting the domains of various kinases of the CK1 kinase family. The percentage amino acid identity within the kinase domains of each kinase to that of CK1 α kinase domain (aa 10-302) is also indicated and the relative similarities potentially define why only CK1 α , α -like, δ and ϵ isoforms but not others interact with FAM83 members.

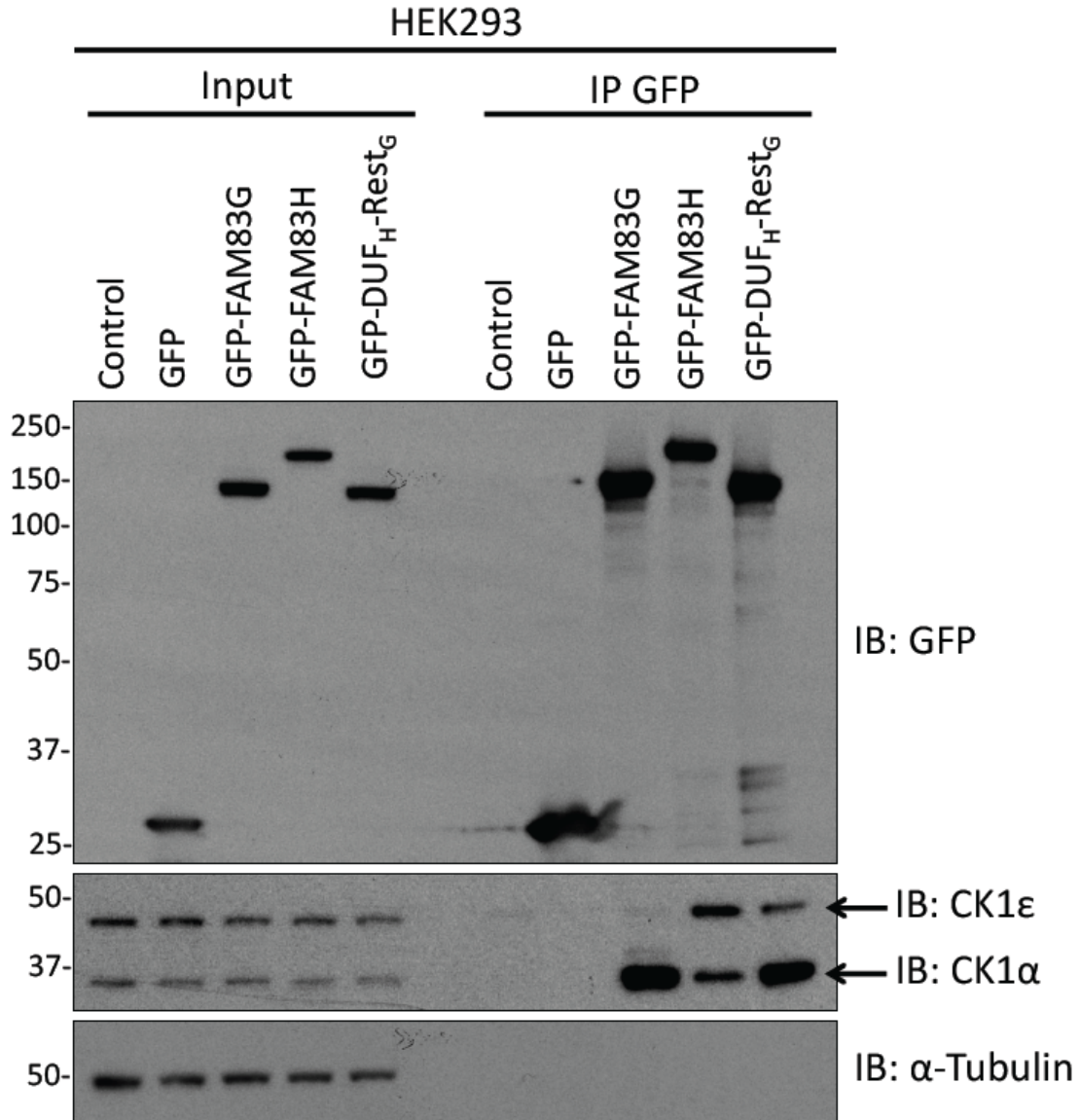


Fig. S5: CK1-specificity switch with *DUF1669* chimera. We switched the GFP-FAM83G *DUF1669* domain, which interacts with CK1 α only, with the *DUF1669* domain of GFP-FAM83H, which interacts with both CK1 α and CK1 ϵ . U20S cells were transfected with this chimera or wild type GFP-tagged constructs. Input extracts and GFP-IPs were resolved by SDS-PAGE, transferred to PVDF membranes and subjected to immunoblotting using the indicated antibodies.

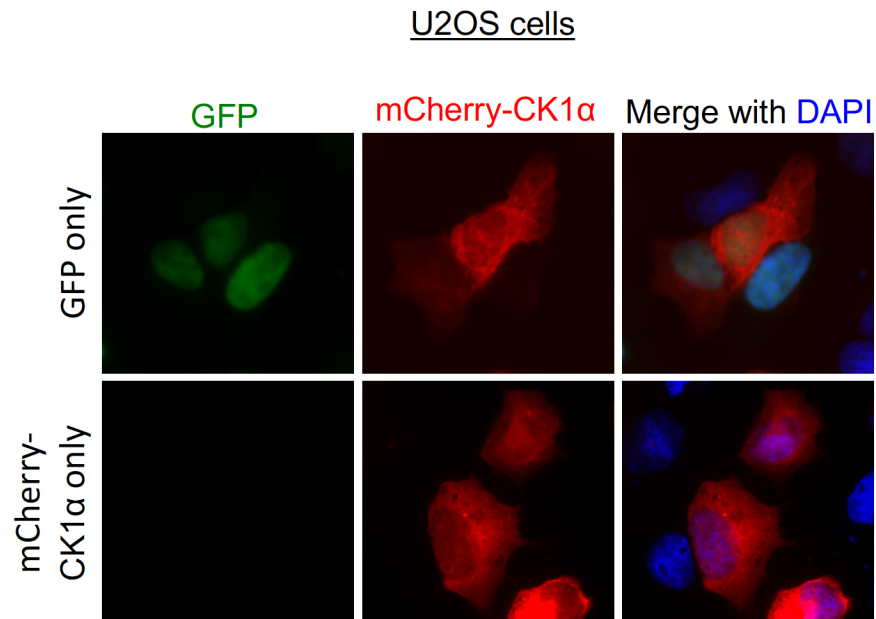


Fig. S6: Fluorescence images of GFP and mCherry-CK1 α controls. U2OS cells stably integrated with Tet-inducible expression of GFP alone were transfected with mCherry-CK1 α . Wild-type U2OS cells were transfected with mCherry-CK1 α as a negative control. GFP expression was induced with doxycycline for 24 h, prior to fixing cells in PFA for fluorescence microscopy. Images were taken using a Nikon TiS inverted microscope. Images were processed using NIS Elements (Nikon) and Adobe Photoshop using identical parameters across all the images. Representative images from one field of view are included. No-overlapping staining between GFP and CK1 α is observed.

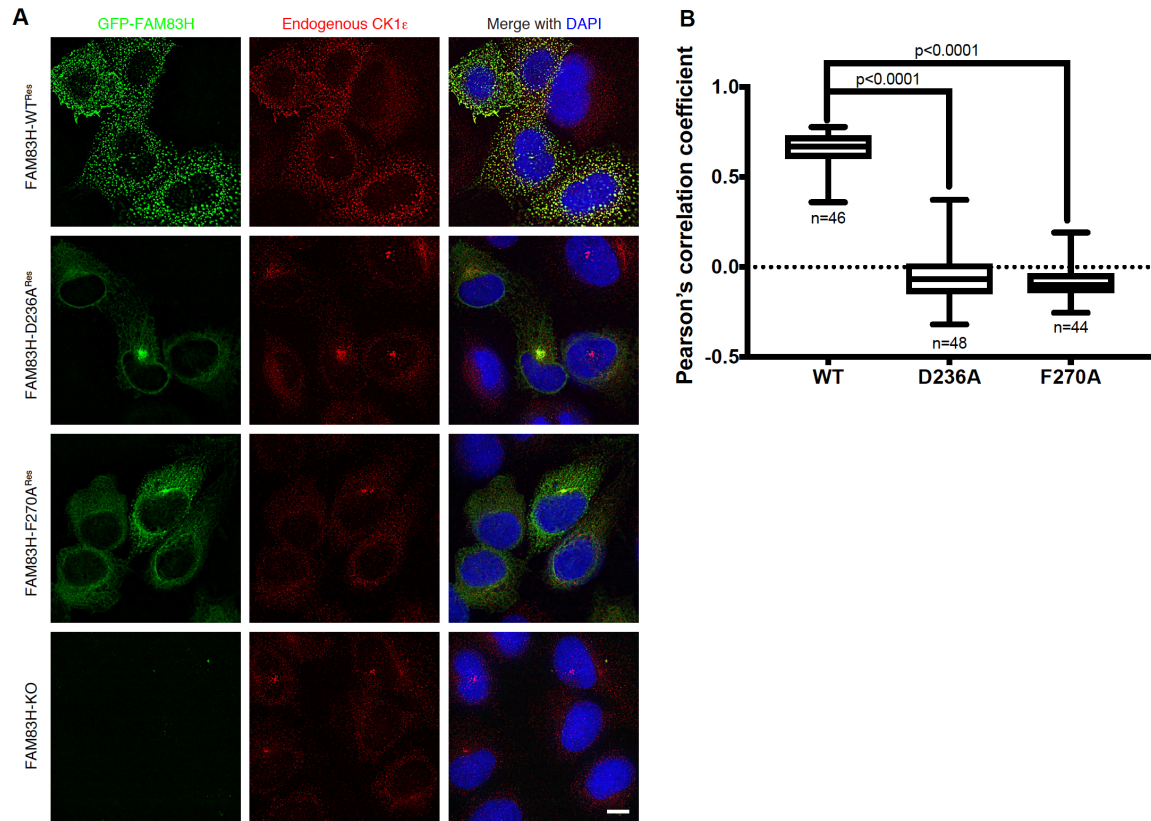
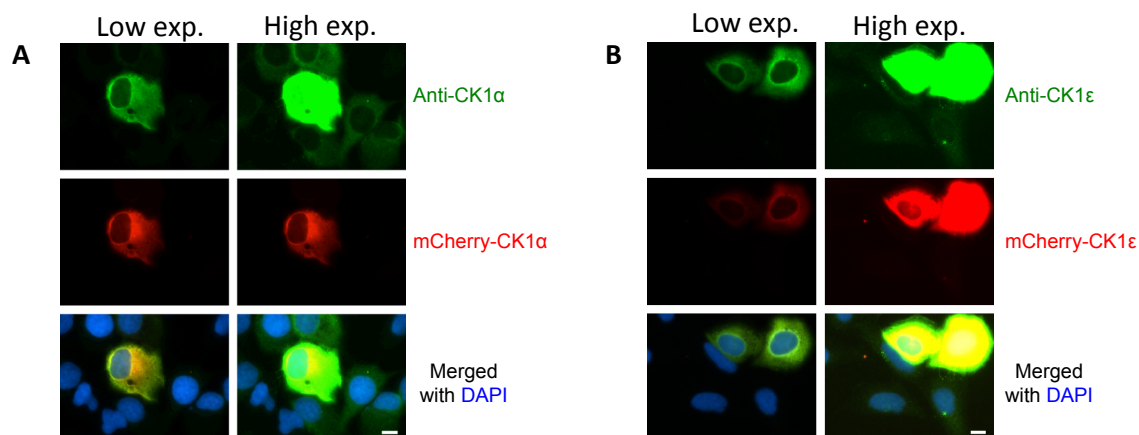


Fig. S7: FAM83H co-localizes with, and in part determines the subcellular localization of, endogenous CK1 ϵ . **A.** FAM83H^{-/-} U2OS cells were transfected with rescue (Res) vectors encoding GFP-FAM83H, GFP-FAM83H-D236A, GFP-FAM83H-F270A mutants or not transfected (FAM83H KO). Cells were fixed in methanol and stained with anti-CK1 ϵ primary antibody and AlexaFluor-594 conjugated secondary antibody. DNA was stained with DAPI. Representative images from one field of view are included. Scale bars represent 10 μ m. **B.** The boxplot shows the range, mean, lower and upper quartile of the Pearson's correlation coefficients of GFP-FAM83H and endogenous CK1 ϵ intensities within above-background pixels in the cytoplasm. Data was obtained from three separate experiments. The mean Pearson's correlation coefficients for different rescue mutants are as follows: FAM83H^{WT}=0.6565, FAM83H^{D236A}=0.05267 and FAM83H^{F270A}=0.01444.



Supplementary Figure 8: Validation of anti-CK1 α and ϵ antibodies for IF applications. **A.** U2OS cells were transfected with mCherry-CK1 α . Cells were fixed in methanol and immuno-stained with anti-CK1 α primary and Alexa-Fluor-488 conjugated secondary antibodies. DNA was stained with DAPI. Fluorescence microscopy images were taken using DeltaVision widefield fluorescence microscope and deconvolved using SoftWorx. Representative low and high exposure images are included. **B.** As in A, except that U2OS cells were transfected with mCherry-CK1 ϵ and stained with anti-CK1 ϵ primary antibodies.

Supplemental Macro for ImageJ added to quantitate co-localization in cells.

```
// ImageJ Macro to calculate colocalization stats for a 3D image stack
// - calculate Pearson Correlation Coefficient (PCC)
// - manual and auto-thresholding options
// - uses a 2D selection as a region of interest throughout stack
//
// Input:
// - image stack containing 2 channels of interest (assumes C1 and C2)
// - provide a 2D ROI to be used throughout the 3D stack
// - specify auto-thresholding method or manual thresholds
//
// Output:
// - thresholded PCC (log window)
// - C1 versus C2 intensity scatter plot
//
// Copyright: g.ball@dundee.ac.uk (2017), Dundee Imaging Facility
// License: Creative Commons CC BY-NC-SA
//
// check input, and reset ROI manager to save input selection
if (selectionType == -1) {
    exit("You must specify a selection!");
}
getDimensions(w, h, nc, nz, nt);
if (nt > 1) {
    exit("Macro does not work with >1 time point! (found" + nt + ")");
}
if (nc < 2) {
    exit("Macro uses first 2 channels! (found only 1)");
}
roiManager("reset");
roiManager("Add");
run("Select None");
// get thresholding method / manual thresholds
Dialog.create("Coloc 3D (ROI) Macro");
threshMethods = newArray("Manual", "Otsu", "Triangle");
Dialog.addChoice("Thresholding method", threshMethods);
Dialog.addNumber("Channel 1 threshold***", 1);
Dialog.addNumber("Channel 2 threshold***", 1);
Dialog.addMessage("*** manual thresholds ignored if auto-thresholding chosen");
Dialog.show();
threshChoice = Dialog.getChoice();
thresh1 = Dialog.getNumber();
thresh2 = Dialog.getNumber();
setBatchMode(true);
// get duplicated single-channel images to work on
getDimensions(w, h, nc, nz, nt);
run("Duplicate...", "duplicate");
baseTitle = getTitle();
run("Split Channels");
selectWindow("C1-" + baseTitle);
idC1 = getImageID();
selectWindow("C2-" + baseTitle);
```

```

idC2 = getImageID();
if (nc > 2) {
    // close unused channels
    for (c = 3; c <= nc; c++) {
        selectWindow("C" + c + "-" + baseTitle);
        close();
    }
}
// 1. create above-threshold mask images for channels 1 and 2
selectImage(idC1); // -- channel 1
run("Select None");
run("Duplicate...", "duplicate");
roiManager("select", 0);
Stack.getStatistics(nVox1, mean1, min1, max1);
min1 = thresh1;
if (threshChoice != "Manual") {
    setAutoThreshold(threshChoice + " dark stack");
    getThreshold(min1, max1);
}
print("Channel 1 threshold = " + min1);
setThreshold(min1, max1);
run("Convert to Mask", "method=Default background=Dark black");
rename("C1-mask");
selectImage(idC2); // -- channel 2
run("Select None");
run("Duplicate...", "duplicate");
roiManager("select", 0);
Stack.getStatistics(nVox2, mean2, min2, max2);
min2 = thresh2;
if (threshChoice != "Manual") {
    setAutoThreshold(threshChoice + " dark stack");
    getThreshold(min2, max2);
}
print("Channel 2 threshold = " + min2);
setThreshold(min2, max2);
run("Convert to Mask", "method=Default background=Dark black");
rename("C2-mask");
// 2. object pixels: inside ROI and above-thresh in channel 1 OR channel 2
imageCalculator("OR create stack", "C1-mask", "C2-mask");
roiManager("select", 0);
setBackground(0, 0, 0);
run("Clear Outside", "stack"); // clear outside ROI!
run("Select None");
rename("object-mask");
idObjects = getImageID();
if (nSlices > 1) {
    Stack.getStatistics(nPixels, mean);
} else {
    getRawStatistics(nPixels, mean);
}
nObj = nPixels * mean / 255; // number of object pixels
print("" + nObj + " object pixels");
i1 = newArray(nObj); // object pixel intensities in channel 1
i2 = newArray(nObj); // object pixel intensities in channel 2
n1 = 0; // temp counter from 0 to nObj for channel 1
n2 = 0; // temp counter from 0 to nObj for channel 2

```



```

// create "binary" array of 0 / 255=object for image stack
selectImage(idObjects);
w = getWidth();
h = getHeight();
nVox = w * h * nSlices;
obj = newArray(nVox);
v = 0;
for (z = 1; z <= nSlices; z++) {
    if (nSlices > 1) {
        Stack.setSlice(z);
    }
    for (y = 0; y < h; y++) {
        for (x = 0; x < w; x++) {
            obj[v] = getPixel(x, y);
            v++;
        }
    }
}
// populate object voxel intensity arrays for channels 1 and 2
v1 = 0; // counter for object voxels in C1 object voxel intensity array
v2 = 0; // counter for object voxels in C2 object voxel intensity array
for (z = 1; z <= nSlices; z++) {
    // channel 1
    selectImage(idC1);
    if (nSlices > 1) {
        Stack.setSlice(z);
    }
    for (y = 0; y < h; y++) {
        for (x = 0; x < w; x++) {
            if (obj[v1] == 255) {
                i1[n1] = getPixel(x, y);
                n1++;
            }
            v1++;
        }
    }
    // channel 2
    selectImage(idC2);
    if (nSlices > 1) {
        Stack.setSlice(z);
    }
    for (y = 0; y < h; y++) {
        for (x = 0; x < w; x++) {
            if (obj[v2] == 255) {
                i2[n2] = getPixel(x, y);
                n2++;
            }
            v2++;
        }
    }
}
}
// clean up and un-hide calculated mask images
selectImage(idC1);
close();
selectImage(idC2);
close();

```

```

setBatchMode("exit and display");
// calculate Object Pearson's coefficient
Array.getStatistics(i1, min1, max1, mean1, std1);
print("Object pixel C1 mean, stdDev = " + mean1 + ", " + std1);
Array.getStatistics(i2, min2, max2, mean2, std2);
print("Object pixel C2 mean, stdDev = " + mean2 + ", " + std2);
rho = 0;
for (i = 0; i < nObj; i++) {
    rho += (i1[i] - mean1) * (i2[i] - mean2);
}
rho = rho / (std1 * std2 * (nObj - 1));
print("Object Pearson coeff, rho = " + rho);
// Plot "Cytofluorogram" (obtain C1, C2 intensities using "List" button)
plotTitle = "Cytofluorogram (for object pixels)";
Plot.create(plotTitle, "C1 intensity", "C2 intensity");
Plot.setLimits(0, max1, 0, max2);
Plot.add("dots", i1, i2);

```